The impulsive response of sandwich beams: analytical and numerical investigation of regimes of behaviour

M.T. Tilbrook, V.S. Deshpande and N.A. Fleck*

Department of Engineering, University of Cambridge, Trumpington Street, Cambridge, CB2 1PZ, UK.

ABSTRACT

An analytical model is developed to classify the impulsive response of sandwich beams based on the relative time-scales of core compression and the bending/stretching response of the sandwich beam. It is shown that an overlap in time scales leads to a coupled response and to the possibility of an enhanced shock resistance. Four regimes of behaviour are defined: decoupled responses with the sandwich core densifying partially or completely, and coupled responses with partial or full core densification. These regimes are marked on maps with axes chosen from the sandwich beam transverse core strength, the sandwich beam aspect ratio and the level of blast impulse. In addition to predicting the times-scales involved in the response of the sandwich beam, the analytical model is used to estimate the back face deflection, the degree of core compression and the magnitude of the support reactions. The predictions of the analytical model are compared with finite element (FE) simulations of impulsively loaded sandwich beams comprising an anisotropic foam core and elastic, ideally plastic face-sheets. The analytical and numerical predictions are in good agreement up to the end of core compression. However, the analytical model under-predicts the peak back face deflection and over-predicts the support reactions, especially for sandwich beams with high strength cores. The FE calculations are employed to construct design charts to select the optimum transverse core strength that either minimises the back face deflections or support reactions for a given sandwich beam aspect ratio or blast impulse. Typically, the value of the transverse core strength that minimises the back face deflection also minimises the support reactions. However, the optimal core strength depends on the level of blast impulse, with higher strength cores required for greater blasts.

Keywords: sandwich beams, blast response, optimization.

Submitted to *J. Mech. Phys Solids,* April 2006

* Corresponding author, Tel.: +44-1223 332650; fax: +44-1223 332662
Email address: naf1@eng.cam.ac.uk

1. Introduction

The blast resistance of structures is of current academic and industrial interest, with sandwich structures being proposed as alternatives to conventional monolithic structures in order to enhance blast resistance. The prototypical problem is sketched in Fig. 1: a planar underwater or air blast impinges a clamped sandwich beam. Several recent studies have shown that sandwich structures subjected to blast loading outperform monolithic structures of equal mass, see for example Fleck and Deshpande (2004) and Xue and Hutchinson (2004). However, the relation between the sandwich core material properties and the sandwich beam performance remains unclear. The aim of this study is to investigate this relationship using analytical and finite element methods.

Fleck and Deshpande (2004) have developed an analytical model for the shock resistance of clamped sandwich beams by separating the response of these beams into three sequential stages: the fluid-structure interaction stage I up to the point of first cavitation of the fluid, the core compression stage II and finally a combined beam bending and stretching stage III. The model of Fleck and Deshpande (2004) temporally decouples the three stages of the sandwich beam responses and provides a framework for understanding the blast response of sandwich beams. The qualitative predictions of the Fleck and Deshpande (2004) analysis for the front face velocity v_f and back face velocity v_b are sketched in Figs. 2a and 2b. The core is taken to be sufficiently strong such that it decelerates the impacted front face and simultaneously accelerates the back face to a common velocity over a time period which is significantly shorter than that of the subsequent co-operative sandwich beam response. The deflection of the back face during the core compression phase (stage II) is also assumed to be small compared to that during the subsequent sandwich beam response. Core compression is either partial or complete: a blast of sufficiently high intensity will cause the front face to slap against the back face with full densification of the core, see Fig. 2b. A low intensity blast, however, will only partially densify the core at the time when v_f drops to the value of v_b, see Fig. 2a.

Recent finite element (FE) simulations by Rabczuk et al. (2005), Liang et al. (2006) and McShane et al. (2006) suggest that the Fleck and Deshpande (2004) model may over-estimate or under-estimate the deflections of the sandwich beams under blast loading. These discrepancies have been attributed to the fact that coupling between the stages of the response can cause enlarged or reduced deflections compared with those predicted by the fully decoupled Fleck and Deshpande (2004) model.

Deshpande and Fleck (2005) have already examined the significance of coupling between the fluid-structure interaction stage I and the core compression stage II. They demonstrated that the Taylor

(1941) analysis based upon a free-standing front face-sheet underestimates by 20% to 40% the transmitted momentum for sandwich beams comprising high strength cores. This analysis was used to explain the discrepancies between the FE simulations of Rabczuk et al. (2005) and the analytical predictions of Fleck and Deshpande (2004). But what is the explanation for the discrepancies indicated by Liang et al. (2006)? McShane et al. (2006) performed FE simulations with the couplings between the three stages of response switched on and off and demonstrated that the enhanced performance for sandwich beams observed in their study and in the study of Liang et al. (2006) is primarily a result of coupling between core compression in Stage II and combined beam bending and stretching in Stage III of the sandwich beam response. This coupling is most significant in beams with a core of low transverse strength.

Liang et al. (2006) have elucidated two types of sandwich response and labelled them as (a) strong core and (b) soft core type responses. The mid-span velocity versus time histories of the front and back faces of the strong core response is the same as that sketched in Fig. 2a: the front and back face velocities equalise early in the deformation history. Subsequently, the faces share a common velocity-time response and both the face-sheets are brought to rest during the subsequent sandwich mode of bending/stretching. In contrast, in the soft core type behaviour (Fig. 2c), the back face begins to *decelerate* while the core is still compressing. Liang et al. (2006) suggest that the optimal performance of sandwich beams is attained for soft core designs. They show that a core with a low transverse strength reduces the transmitted impulse during the initial fluid-structure interaction stage. Also the coupling is increased between the core compression stage (II) and the combined beam bending and stretching stage (III) of the sandwich beam response. However, sandwich cores of very low strength will fully densify and this will not only result in a loss in bending strength of the sandwich beams but also give rise to very high support reactions when the front face slams into the back face. A major objective of the current study is to explain the findings of Liang et al. (2006) in terms of the relative timescales for core compression, the dynamic response of the back face and the overall sandwich beam response.

The three-dimensional FE studies of Liang et al. (2006) and McShane et al. (2006) investigated the blast response of sandwich beams with specific core topologies such as the square-honeycomb or Y-frame. While these studies have demonstrated the possible beneficial effects of cores with low transverse strength, the precise relation between the core strength and blast resistance of sandwich beams remains unclear. The present study focuses on understanding this relation for impulsively loaded sandwich beams. Rather than addressing a particular core topology, a uniform but anisotropic core material is adopted whose properties in each direction may be varied independently. McShane et

al. (2006) have already demonstrated that the coupling between the core compression and the beam bending/stretching phases has the most significant effect on the sandwich beam response. Thus, we restrict the current study to an investigation of the blast the response of sandwich beams with the effects of fluid-structure interaction neglected, i.e. we shall study impulsively loaded beams.

Scope of study

The main aims of this study are to:

(i) Develop an analytical model for the impulsive response of sandwich beams accounting for possible couplings between the core compression and beam bending/stretching phases.

(ii) Use this analytical model to construct maps showing the regimes of behaviour of the sandwich beams.

(iii) Compare the analytical and FE predictions of the impulsive response of sandwich beams over all regimes of behaviour.

(iv) Use the FE simulations to determine the optimal core strength that maximises blast resistance of the sandwich beam.

2. Analytical model for impulsive loading of sandwich beams

Consider a sandwich beam of span $2L$, core thickness c and front and back face-sheets of thicknesses h_f and h_b, respectively. The core of density ρ_c is made from a rigid-ideally plastic compressible solid with uniaxial yield strengths σ_t and σ_l in the through-thickness transverse and longitudinal directions, respectively. (The tensile and compressive yield values are taken to be equal.) The foam-like core is assumed to have a nominal compressive densification strain ε_D in the transverse direction: beyond the densification strain no additional transverse plastic strain can accumulate within the core. The face-sheet material has a density ρ_f and is also assumed to be rigid-ideally plastic with a tensile strength σ_Y. The boundary conditions for the sandwich beam are sketched in Fig. 1. The back face is fully clamped at two outer supports while only the lateral displacements of the front face are constrained. These boundary conditions were previously employed by Liang et al. (2006) and are considered to be representative of ship hulls when the bulk-heads do not extend to the outer face. This sandwich beam is impulsively loaded with an impulse I per unit length applied uniformly to the front face-sheet of the sandwich beam.

In the following analysis we relax the simplifying approximation of decoupling the response into sequential stages, as in Fleck and Deshpande (2004). Rather, we analyze the motions of the front and back faces separately using a lumped mass approximation with the mass of the core assumed to be distributed equally and uniformly over the front and back face-sheets. Further, we neglect any strengthening of the core due to micro-inertial or shock wave effects and assume that the transverse compressive strength σ_t loads the back face and decelerates the front face as illustrated in Fig. 3. This analysis holds until the velocities of the front and back faces equalise. After the face-sheet velocities have equalised, sandwich action follows and finally the motion arrests. A critical assumption in this analysis is that we neglect the shear strength of the core prior to equalisation of the velocities of the front and back faces but then allow for sandwich action (which implies a finite shear strength) upon equalisation of the face-sheet velocities. The validity of this assumption is confirmed via full FE simulations in Section 3.

2.1 Governing equations prior to equalisation of the face-sheet velocities

We first develop the governing equations for the motion of the front and back faces of the sandwich beam by employing the model sketched in Fig. 3. In this initial phase of motion the front and back face-sheets act independently and thus this analysis is only valid prior to equalisation of the face-sheet velocities. Employing the lumped mass approximation, the mass per unit length of the front and back faces are

$$m_f = h_f \rho_f + \rho_c c/2\,, \tag{1a}$$

and

$$m_b = h_b \rho_f + \rho_c c/2\,, \tag{1b}$$

respectively. With an impulse I applied uniformly to the front face of the sandwich beam, the initial velocity v_o of the front face in this lumped mass model follows as

$$v_o = \frac{I}{m_f}\,. \tag{2}$$

2.1.1 Front face

The front face is constrained to move in the transverse direction (x_2-direction) and is decelerated from its initial velocity v_o by a constant pressure σ_t due to the finite transverse strength of the core. Thus, at time t the velocity v_f and displacement w_f of the front face are given by

$$v_f(t) = v_o - \frac{\sigma_t}{m_f} t\,, \tag{3}$$

and

$$w_f(t) \equiv \varepsilon(t)c = v_o t - \frac{\sigma_t}{2m_f} t^2, \qquad (4)$$

respectively, where ε is the nominal core strain at the supports. Recall that the nominal compressive strain in the core cannot exceed ε_D. Full densification of the core will occur first at the supports, at a time t_D given from Eq. (4) as

$$t_D = \frac{m_f v_o}{\sigma_t} - \sqrt{\left(\frac{m_f v_o}{\sigma_t}\right)^2 - \frac{2m_f \varepsilon_D c}{\sigma_t}}. \qquad (5)$$

Now examine the term inside the square root sign of (5). For the choice $m_f v_o^2 < 2\sigma_t \varepsilon_D c$, the kinetic energy of the face-sheet is sufficiently low for the core to not fully densify and $t_D = \infty$. Note that $m_f v_o^2 > 2\sigma_t \varepsilon_D c$ is the necessary condition for full core densification at the supports. However, this condition is not sufficient: if the face-sheet velocities equalise at mid-span at a time less than t_D, it is assumed that core compression halts along the whole length of the beam, and sandwich action commences before full densification is achieved at the supports.

2.1.2 Back face

The back face is modelled as a clamped monolithic beam of mass per unit length m_b, initially at rest and loaded with a uniform transverse pressure σ_t. This is a classical problem and has already been analysed by Jones (1989) using a small deflection assumption. Here we develop a finite deflection solution along the lines of the impulsive solution of Fleck and Deshpande (2004). We assume that yield of the back face is attained when the longitudinal force N and bending moment M satisfy one or both of the relations

$$|N| = N_b \quad \text{and} \quad |M| = M_b. \qquad (6)$$

where $M_b \equiv \sigma_Y h_b^2/4$ is the plastic bending moment and $N_b \equiv \sigma_Y h_b$ is the longitudinal plastic stretching force. As noted by Jones (1989), the response of this clamped monolithic beam depends on the transverse pressure σ_t acting from the core onto the back face, and solutions are obtained for the following three cases.

Case I: High strength core, such that $\sigma_t > 3\frac{\sigma_Y h_b^2}{L^2}$

The transverse motion of the beam is separated into two sequential phases as in the small displacement analysis of Jones (1989). In the initial phase I (Fig. 4a), the central portion of the beam translates at a velocity

$$v_b = \frac{\sigma_t}{m_b} t, \qquad (7a)$$

resulting in a displacement

$$w_b = \frac{\sigma_t}{2m_b} t^2 . \qquad (7b)$$

At each end of the beam, a segment of length ξ rotates about the supports. The bending moment varies from $-M_b$ at the outer stationary plastic hinge at the supports to M_b at the ends of the segments of length ξ. For the assumed velocity field (Fig. 4a), the shear force is zero over the central section and this sets $M = M_b$ over the entire central section. Increments in curvature occur only at the ends of the rotating segments while axial straining is distributed over the length of the rotating segments. A free body diagram for half the clamped back face is shown in Fig. 4b. Conservation of moment of momentum about a fixed end after a time t gives

$$m_b v_b (L-\xi)\left(\xi + \frac{L-\xi}{2}\right) + \int_0^{\xi} \frac{m_b v_b x^2}{\xi} \mathrm{d}x = \frac{\sigma_t L^2}{2} t - 2M_b t - N_b \int_0^t w_b \mathrm{d}t , \qquad (8)$$

where x is the axial co-ordinate from one end of the beam as shown in Fig. 4a. This equation gives ξ as a function of time as

$$\xi = \sqrt{\frac{12M_b}{\sigma_t} + \frac{N_b t^2}{m_b}} , \qquad (9)$$

indicating that the hinges form at $\xi_o = \sqrt{\frac{3\sigma_Y h_b^2}{\sigma_t}}$ at time $t = 0$. The assumed velocity field is only valid for $\xi_o < L$ and consequently this solution is only valid for $\sigma_t > 3\frac{\sigma_Y h_b^2}{L^2}$.

Phase I continues until the travelling hinges at the inner ends of the segments of length ξ coalesce at $\xi = L$. Thus, from Eq. (9), phase I ends at time t_I

$$t_I = \sqrt{\frac{m_b}{N_b}\left(L^2 - \frac{12M_b}{\sigma_t}\right)} . \qquad (10)$$

The velocity and displacement of the mid-span of the back face at this time are given by

$$v_b^I = \frac{\sigma_t}{m_b} t_I , \qquad (11a)$$

and

$$w_b^I = \frac{\sigma_t}{2m_b} t_I^2 , \qquad (11b)$$

respectively.

7

In phase II of the motion, stationary plastic hinges exist at the mid-span and at the ends of the beam, with the moment varying from $-M_b$ at the beam end to M_b at mid-span. The velocity profile is triangular, as sketched in Fig. 4c and the equation of motion for moderate deflections follows from the free-body diagram sketched in Fig. 4d as

$$\frac{\sigma_t L^2}{2} - 2M_b - N_b w_b = \frac{\ddot{w}_b}{L}\int_0^L m_b x^2 \mathrm{d}x, \qquad (12)$$

where x is the axial co-ordinate from one end of the beam as shown in Fig. 4d, and the over-dot denotes differentiation with respect to time. With initial conditions $w_b(t_I) = w_b^I$ and $\dot{w}_b(t_I) = v_b^I$, this differential equation admits a solution of the form

$$w_b(t) = \frac{v_b^I}{\omega}\sin\left[\omega(t-t_I)\right] - \frac{4M_b}{N_b}\cos\left[\omega(t-t_I)\right] + \left(\frac{4M_b}{N_b} + w_b^I\right), \qquad (13a)$$

where

$$\omega = \frac{1}{L}\sqrt{\frac{3N_b}{m_b}}. \qquad (13b)$$

Thus, the velocity of the back face at mid-span at times $t > t_I$ is given by

$$v_b = \dot{w}_b = v_b^I \cos\left[\omega(t-t_I)\right] + \frac{4M_b}{N_b}\omega\sin\left[\omega(t-t_I)\right]. \qquad (14)$$

The time t_{bd} at which the back face begins to decelerate is obtained by setting $\dot{v}_b = 0$ in Eq. (14), to give

$$t_{bd} = t_I + \frac{1}{\omega}\tan^{-1}\left(\frac{4M_b\omega}{N_b v_b^I}\right), \qquad (15)$$

while the back face arrests ($v_b = 0$) after

$$t_{bs} = t_I + \frac{1}{\omega}\left[\frac{\pi}{2} + \tan^{-1}\left(\frac{4M_b\omega}{N_b v_b^I}\right)\right]. \qquad (16)$$

And now a word of caution. The solution based on Eq. (12) is only valid for moderate transverse deflections. For very large values of σ_t (outside the regime of practical relevance) the back face motion does not arrest.

Case II: Intermediate strength core, such that $\dfrac{\sigma_Y h_b^2}{L^2} < \sigma_t \le 3\dfrac{\sigma_Y h_b^2}{L^2}$

In this parameter range, phase I does not exist and motion of the back face commences in phase II, with stationary plastic hinges existing at mid-span and at the ends of the beam. The governing equation for motion of the back face is Eq. (12) with initial conditions $w_b(0) = \dot{w}_b(0) = 0$. Thus, the mid-span deflection and velocity of the back face are given by

$$w_b = \left(\frac{\sigma_t L^2 - 4M_b}{2N_b} \right)(1 - \cos \omega t), \tag{17a}$$

and

$$v_b = \omega \left(\frac{\sigma_t L^2 - 4M_b}{2N_b} \right) \sin \omega t, \tag{17b}$$

respectively, while the times t_{bd} and t_{bs} are specified by

$$t_{bd} = \frac{\pi}{2} L \sqrt{\frac{m_b}{3N_b}}, \tag{18a}$$

and

$$t_{bs} = \pi L \sqrt{\frac{m_b}{3N_b}}, \tag{18b}$$

respectively.

Case III: Low strength core, such that $\sigma_t \le \frac{\sigma_Y h_b^2}{L^2}$

According to Eq. (12) a core of low transverse strength ($\sigma_t \le \frac{\sigma_Y h_b^2}{L^2}$) will not deform the back face. Thus, within the rigid-ideally plastic idealisation, the back face does not deflect due to the pressure σ_t exerted by the core, and we have $w_b = \dot{w}_b = 0$, $t_{bd} = t_{bs} = \infty$.

2.2 End of core compression

In Section 2.1 we have developed the governing equations for motion of the front and back faces by assuming that the two face-sheets deflect independently. After core compression ends the faces move co-operatively and sandwich action dominates the response. Following Fleck and Deshpande (2004) we assume that sandwich action commences at the time t_{eq} when core compression ends. Now core compression ends when the core has densified at the supports, at $t = t_D$, or when the front and back face-sheet velocities are equal at the mid-span, whichever occurs first. The velocity and displacement of the front face over the period $0 \le t \le t_{eq}$ are given by Eqs. (3) and (4), respectively, and we proceed to determine t_{eq} for the three cases considered in Section 2.1.

Case I: $\sigma_t > 3\frac{\sigma_Y h_b^2}{L^2}$

In order to calculate the end of core compression, we compare the mid-span velocities of the front and back faces. Equalization of the velocities of the faces in this case can occur in the following three

9

scenarios: (a) during phase I of the back face; (b) during phase II of the back face; or (c) after motion of the back face has ceased.

Case I(a): *Core compression ends during phase I of the back face motion.*
In phase I of the motion of the back face, v_b is given by Eq. (7a). Upon equating v_b to v_f from Eq. (3), we obtain the time θ_I where

$$\theta_I = \frac{v_o m_b m_f}{\sigma_t (m_b + m_f)}. \tag{19}$$

For this solution to be valid we require that $\theta_I \le t_I$. Core compression ends during phase I of the back face motion provided

$$t_{eq} \equiv \min(\theta_I, t_D) \le t_I, \tag{20}$$

where $\min(x_1, x_2)$ is the minimum value of either x_1 or x_2. If this inequality is not met, then core compression continues into phase II of the back face motion.

Suppose that the core compression ends at t_{eq} during phase I of the back face motion. Then the linear momentum of the entire sandwich beam over the duration $0 \le t \le t_{eq}$ follows as

$$p = 2\left[m_f L v_o - \frac{\xi}{2}\sigma_t t \right], \tag{21}$$

where the length ξ of the rotating segment on the back face is given by Eq. (9). The momentum changes due to the reaction force at each of the supports,

$$R = -\frac{\dot{p}}{2} = \frac{\xi \sigma_t}{2} + \frac{\sigma_t N_b t^2}{2 m_b \xi}, \tag{22}$$

while the deflection of mid-span of the back face is given by Eq. (7b). The linear momentum of the entire sandwich beam at the end of core compression $t = t_{eq}$ is given by

$$p_{eq} = 2\left[m_f L v_o - \frac{\xi_{eq}}{2}\sigma_t t_{eq} \right], \tag{23}$$

where ξ_{eq} is given by substituting $t = t_{eq}$ in Eq. (9). The mid-span deflection of the back face at this time is

$$w_b^{eq} = \frac{\sigma_t}{2m_b} t_{eq}^2 . \tag{24}$$

The nominal core compression strain at the mid-span and supports at this instant are obtained from the deflections of the front and back face as

$$\varepsilon_m = \frac{v_o t_{eq}}{c} - \frac{\sigma_t t_{eq}^2}{2c}\left(\frac{1}{m_f} + \frac{1}{m_b} \right), \tag{25a}$$

and

$$\varepsilon_s = \frac{v_o t_{eq}}{c} - \frac{\sigma_t t_{eq}^2}{2cm_f}, \tag{25b}$$

respectively.

Case I(b): *Core compression ends during phase II of the back face motion.*
The front face velocity v_f as given by Eq. (3) equals the back face velocity v_b as given by Eq. (14) after a time θ_{II}, obtained by solving the implicit equation

$$v_o - \frac{\sigma_t}{m_f}\theta_{II} = v_b^I \cos[\omega(\theta_{II} - t_I)] + \frac{4M_b}{N_b}\omega \sin[\omega(\theta_{II} - t_I)]. \tag{26a}$$

For this solution to be valid we require that $t_I < \theta_{II} \le t_{bs}$. Core compression ends during phase II when

$$t_I < t_{eq} \equiv \min(\theta_{II}, t_D) \le t_{bs}. \tag{26b}$$

If neither inequality (20) nor (26b) is satisfied, then core compression continues after the back face has arrested.

Suppose that core compression ends during phase II of the back face motion. The velocity and displacement of the back face over the duration $0 \le t \le t_I$ are given by Eqs. (7a) and (7b), respectively, while the linear momentum and the support reactions are specified by Eqs. (21) and (22) for $t \le t_I$. Over the period $t_I < t \le t_{eq}$, the linear momentum of the beam is

$$p = 2\left[m_f L\left(v_o - \frac{\sigma_t}{m_f} t \right) + \frac{m_b L}{2} v_b^I \cos[\omega(t - t_I)] + \frac{4M_b}{N_b}\omega \sin[\omega(t - t_I)] \right], \tag{27}$$

while the support reaction is

$$R = L\sigma_t + \frac{m_b L \omega}{2} v_b^I \sin[\omega(t - t_I)] - \frac{4M_b}{N_b}\omega^2 \cos[\omega(t - t_I)]. \tag{28}$$

During phase II, the mid-span back face deflection and velocity are given by Eqs. (13) and (14), respectively. At the end of core compression, the momentum p_{eq} of the entire sandwich beam and the mid-span back face deflection w_b^{eq} are given by substituting $t = t_{eq}$ into Eqs. (27) and (13a), respectively. The core compression at mid-span and at the supports then follow as

$$\varepsilon_m = \frac{1}{c}\left[v_o t_{eq} - \frac{\sigma_t}{2m_f} t_{eq}^2 - w_b^{eq} \right], \tag{29a}$$

and

$$\varepsilon_s = \frac{1}{c}\left[v_o t_{eq} - \frac{\sigma_t}{2m_f} t_{eq}^2 \right], \tag{29b}$$

respectively.

Case I(c): *Core compression ends after the arrest of the back face.*
The front face arrests at a time θ_{III}. This time is determined by setting $v_f = 0$ in Eq. (3, to obtain

$$\theta_{III} = \frac{m_f v_o}{\sigma_t}. \tag{30a}$$

Core compression ends after arrest of the back face provided

$$t_{eq} \equiv \min(\theta_{III}, t_D) > t_{bs}. \tag{30b}$$

The support reaction, mid-span back face velocity and deflection over the duration $0 \le t \le t_1$ are given by Eqs. (22), (7a) and (7b), respectively, while w_b, v_b and R are specified by Eqs. (13), (14) and (28) over the duration $t_1 < t \le t_{bs}$. The support reaction is $R = \sigma_t L$ over the duration $t_{bs} < t \le t_{eq}$. Further, as $v_b = 0$ during this period the deflection $w_b = w_b^{eq}$ is given by substituting $t = t_{bs}$ into Eq. (13). The momentum of the entire sandwich beam at the end of core compression is

$$p_{eq} = 2Lm_f\left(v_o - \frac{\sigma_t}{m_f}t_{eq}\right), \tag{31}$$

while the degree of core compression at the mid-span and supports are given by Eqs. (29a) and (29b), respectively.

Case II: $\dfrac{\sigma_Y h_b^2}{L^2} < \sigma_t \le 3\dfrac{\sigma_Y h_b^2}{L^2}$

Equalization of the velocities of the faces at mid-span can occur (a) while the back face is in motion or (b) after the motion of the back face has ceased.

Case II(a): *End of core compression while the back face is in motion*
The time θ at which v_f, given by Eq. (3), equals v_b, given by Eq. (17b), is obtained by solving the following implicit equation

$$\omega\left(\frac{\sigma_t L^2 - 4M_b}{2N_b}\right)\sin\omega\theta = v_o - \frac{\sigma_t}{m_f}\theta. \tag{32}$$

For this solution to be valid we require that $0 < \theta \le t_{bs}$. Core compression ends when

$$0 < t_{eq} \equiv \min(\theta, t_D) \le t_{bs}. \tag{33}$$

If this condition is not met, then core compression continues after the back face has arrested.

The linear momentum of the sandwich beam and the support reaction over the duration $0 \le t \le t_{eq}$ follow as

$$p = 2\left[m_f L\left(v_o - \frac{\sigma_t}{m_f} t \right) + \frac{m_b \omega L}{2}\left(\frac{\sigma_t L^2 - 4M_b}{2N_b} \right)\sin \omega t \right], \qquad (34)$$

and

$$R = L\sigma_t - \frac{m_b L \omega^2}{2}\left(\frac{\sigma_t L^2 - 4M_b}{2N_b} \right)\cos \omega t\,, \qquad (35)$$

respectively. The mid-span back face deflection and velocity are given by Eqs. (13) and (14), respectively, while the deflection w_b^{eq} and momentum p_{eq} are given by substituting $t = t_{eq}$ into Eqs. (17a) and (34), respectively. Note that the core compression at the mid-span and supports is again given by Eq. (29).

Case II(b): *Core compression ends subsequent to arrest of the back face.*
The front face arrests at a time θ_{III} given by Eq. (30a) and this solution is valid if $\theta_{III} > t_{bs}$. Core compression ends at t_{eq} given by Eq. (30b). Over the duration $0 \le t \le t_{bs}$, the support reactions, the mid-span back face velocity and deflections are given by Eqs. (35), (13) and (14), respectively. No further back face deflection occurs over the period $t_{bs} < t \le t_{eq}$ with $w_b = w_b^{eq}$ given by substituting $t = t_{bs}$ in Eq. (17a) and $v_b = 0$. The momentum of the entire sandwich beam at the end of core compression is given by Eq. (31) while the core compression at mid-span and supports is given by Eq. (29).

Case III: $\sigma_t \le \dfrac{\sigma_Y h_b^2}{L^2}$

Recall that in this case the transverse compressive strength of the core is insufficient to initiate deformation in the back face. Equalisation of the front and back face velocities occurs at t_{eq} either (a) if the motion of the front face ceases, or (b) if core densification occurs. Thus, t_{eq} is given by Eq. (30a) and the momentum p_{eq} is given by Eq. (31). The mid-span back face deflection w_b and velocity v_b are identically zero over the duration $0 \le t \le t_{eq}$ and the core compression is again given by Eq. (29).

2.3 The sandwich phase of motion

The core compression ends at time $t = t_{eq}$ and, as discussed in Section 2.2, the beam has a residual momentum p_{eq} with a mid-span back face deflection w_b^{eq}. We assume that sandwich action involving

the co-operative motion of the front and back faces commences at this instant. Here we present a "modal" estimate for subsequent deformation of the sandwich beam. We neglect any travelling hinge phases in the sandwich beam and assume a velocity profile as in Fig. 4c involving stationary plastic hinges at the mid-span and supports of the sandwich beam. An alternative assumption could have been to assume that the front face at $t = t_{eq}$ adopts the velocity profile of the back face. In either case, while we conserve the total linear momentum, a sudden change in the spatial velocity distribution of the two faces is, in general, inevitable. For simplicity we assume the modal solution for $t > t_{eq}$.

Similar to the monolithic back face considered in Section 2.1, we assume that the yield locus of the sandwich beam is approximated by a square described by

$$| N |= N_s \quad \text{and} \quad | M |= M_s \ , \tag{36a}$$

at the supports and

$$| N |= N_s \quad \text{and} \quad | M |= M_m \ , \tag{36b}$$

at mid-span. Here N_s is plastic value of the longitudinal force of the sandwich beam and M_s and M_m are the plastic bending moments at the supports and mid-span, respectively. (Recall that the compressed sandwich beam has a non-uniform depth with compressive core strains ε_m and ε_s at the mid-span and supports, respectively, as illustrated in Fig. 5b) While the plastic value of the longitudinal force

$$N_s = (h_f + h_b)\sigma_Y + \sigma_l c \, , \tag{37}$$

is assumed to be constant over the length of the sandwich beam, the plastic bending moments at the mid-span and supports differ. In the compressed state, the plastic neutral axis of the sandwich beam is at a distance $z_m + c(1\text{-}\varepsilon_m)/2$ and $z_s + c(1\text{-}\varepsilon_s)/2$ below the front face sheet at the mid-span and supports respectively (Fig. 5b), where

$$z_m = \frac{\sigma_Y (1 - \varepsilon_m)}{2\sigma_l}(h_b - h_f) \tag{38a}$$

and

$$z_s = \frac{\sigma_Y (1 - \varepsilon_s)}{2\sigma_l}(h_b - h_f) \, . \tag{38b}$$

Thus, the plastic bending moment of the sandwich beam section at the mid-span and supports is given by

$$\begin{aligned} M_m = {} & \sigma_Y h_f \left[\frac{c(1-\varepsilon_m)}{2} + z_m + \frac{h_f}{2} \right] + \sigma_Y h_b \left[\frac{c(1-\varepsilon_m)}{2} - z_m + \frac{h_b}{2} \right] \\ & + \frac{\sigma_l}{2(1-\varepsilon_m)} \left[\frac{c(1-\varepsilon_m)}{2} + z_m \right]^2 + \frac{\sigma_l}{2(1-\varepsilon_m)} \left[\frac{c(1-\varepsilon_m)}{2} - z_m \right]^2 , \end{aligned} \tag{39a}$$

and

$$M_s = \sigma_Y h_f\left[\frac{c(1-\varepsilon_s)}{2}+z_s+\frac{h_f}{2}\right]+\sigma_Y h_b\left[\frac{c(1-\varepsilon_s)}{2}-z_s+\frac{h_b}{2}\right] + \frac{\sigma_l}{2(1-\varepsilon_s)}\left[\frac{c(1-\varepsilon_s)}{2}+z_s\right]^2+\frac{\sigma_l}{2(1-\varepsilon_s)}\left[\frac{c(1-\varepsilon_s)}{2}-z_s\right]^2, \tag{39b}$$

respectively. Recall that the sandwich phase of motion begins when core compression ends at the supports and thus we take the reference section for the subsequent deflection to be at the supports and w is defined as the deflection of the plastic neutral axis of the sandwich beam at mid-span with respect to the stationary plastic neutral axis at the supports, as shown in Figs. 5b and 5c. The equation of motion of the half sandwich beam sketched in Fig. 5c is then given by

$$(M_s+M_m)+N_s w=-\frac{\ddot{w}}{L}\int_0^L(m_b+m_f)x^2\mathrm{d}x=-\frac{\ddot{w}}{3}(m_b+m_f)L^2, \tag{40}$$

Conserving the total linear momentum of the beam at $t=t_{eq}$, the initial conditions for Eq. (40) are

$$w(t_{eq})\equiv w_s=\frac{w_b^{eq}}{2}+\left(z_m - z_s\right), \tag{41a}$$

and

$$\dot{w}(t_{eq})\equiv v_s=\frac{p_{eq}}{(m_f+m_b)L}. \tag{41b}$$

Equation (40) then admits a solution of the form

$$w=\frac{v_s}{\omega_s}\sin\left[\omega_s(t-t_{eq})\right]+\left(\frac{M_s+M_m}{N_s}+w_s\right)\cos\left[\omega_s(t-t_{eq})\right]-\frac{M_s+M_m}{N_s}, \tag{42a}$$

where

$$\omega_s=\frac{1}{L}\sqrt{\frac{3N_s}{m_f+m_b}}, \tag{42b}$$

and the deflection of the back face of the sandwich beam is

$$w_b(t)=(w-w_s)+w_b^{eq}. \tag{42c}$$

The maximum deflection at mid-span of the sandwich beam occurs at the time when $\dot{w}(T)=0$. Upon substituting this termination condition into the time derivative of Eq. (42a), the response time is obtained as

$$T=t_{eq}+\frac{1}{\omega_s}\tan^{-1}\left[\frac{N_s v_s}{\omega_s(M_m+M_s+w_s N_s)}\right], \tag{43}$$

and the corresponding maximum deflection of the back face at mid-span is

$$W_b=w_b^{eq}+\sqrt{\frac{v_s^2}{\omega_s^2}+\left(\frac{M_s+M_m}{N_s}+w_s\right)^2}-\left(\frac{M_m+M_s}{N_s}+w_s\right). \tag{44}$$

15

With the linear momentum of the sandwich beam for the duration $t_{eq} \le t \le T$ given by

$$p = (m_b + m_f)L\left[v_s \cos\left[\omega_s (t - t_{eq})\right] - \left(\frac{M_s + M_m}{N_s} + w_s \right)\omega_s \sin\left[\omega_s (t - t_{eq})\right]\right], \quad (45)$$

the transient reaction force at the supports follows as

$$R = \frac{L}{2}(m_b + m_f)\left[v_s \omega_s \sin\left[\omega_s (t - t_{eq})\right] + \left(\frac{M_s + M_m}{N_s} + w_s \right)\omega_s^2 \cos\left[\omega_s (t - t_{eq})\right]\right]. \quad (46)$$

During the sandwich phase, the front and back faces have equal velocities with their mid-span velocities given by

$$v_b = v_f = \dot{w} = v_s \cos\left[\omega_s (t - t_{eq})\right] - \omega_s \left(\frac{M_s + M_m}{N_s} + w_s \right)\sin\left[\omega_s (t - t_{eq})\right]. \quad (47)$$

It is recognised that the modal solution will under-predict the deflections and the response time (and consequently over-predict the support reaction force). The significance of this deficiency of the model will be assessed by comparisons with finite element predictions presented in Section 3.

2.4 Regimes of behaviour

The finite element calculations of Liang et al. (2006) have indicated two distinct types of front and back face velocity versus time histories as sketched in Fig. 2. In Figs. 2a and 2b the front and back face velocities equalize while the back face is still accelerating. This is essentially the situation modelled by the decoupled analysis of Fleck and Deshpande (2004) and we shall refer to this as the decoupled regime. A scenario where the velocities of the back and front face equalize subsequent to the back face attaining its maximum velocity is sketched in Fig. 2c. In such a regime, the core compression phase is strongly coupled with the combined bending and stretching of the back face. We shall refer to this regime as the coupled regime. Additionally, we note that complete densification of the core can occur at the supports resulting in the sudden equalization of the velocities of the front and back faces. This sudden equalization can occur either before or after the back face has attained its maximum velocity. Thus, the regimes of behaviour of the sandwich beam can be defined by comparing various times-scales in the response and are summarized as:

Regime A: Decoupled response with partial core densification:

$$t_{eq} < t_D \text{ and } t_{eq} < t_{bd}. \quad (48a)$$

Regime B: Decoupled regime with full core densification:

$$t_{eq} = t_D \text{ and } t_{eq} < t_{bd}. \quad (48b)$$

Regime C: Coupled response with partial core densification:

$$t_{eq} < t_D \text{ and } t_{eq} > t_{bd}. \quad (48c)$$

Regime D: Coupled response with full core densification:

$$t_{eq} = t_D \text{ and } t_{eq} > t_{bd}. \qquad (48d)$$

We note that sandwich beams with $\sigma_t < \sigma_Y h_b^2 / L^2$ always lie in the decoupled regime as no back face bending occurs during core compression. In such a case, the response will either end with partial core densification and no back face deflection (regime A) or full core densification followed by the sandwich phase (regimes B).

Schematics of the typical mid-span front and back face velocity versus time histories in each of these four regimes are sketched in Fig. 6. Recall that Liang et al. (2006) had classified the types of responses they observed into the soft and hard core type responses. While they did not quantify the distinction between these two types of behaviour we note that the decoupled regime with partial densification (regime A) and the coupled regime with partial densification (regime C) are essentially consistent with the hard and soft core type responses, respectively, as described by Liang et al. (2006).

2.5 Non-dimensional groups

The above equations can all be presented in terms of non-dimensional groups. For the sake of brevity, we do not present the non-dimensional forms here. Rather, we introduce the relevant independent and dependent non-dimensional groups and present all subsequent results in terms of these groups.

The non-dimensional geometric variables of the sandwich beam are

$$\bar{c} \equiv \frac{c}{L}, \quad \bar{h} \equiv \frac{h_f + h_b}{2c} \text{ and } \hat{h} \equiv \frac{h_b}{h_f}, \qquad (49a)$$

and the non-dimensional core properties are

$$\bar{\rho} \equiv \frac{\rho_c}{\rho_f}, \quad \bar{\sigma}_l \equiv \frac{\sigma_l}{\bar{\rho}\sigma_Y}, \bar{\sigma}_t \equiv \frac{\sigma_t}{\bar{\rho}\sigma_Y} \text{ and } \varepsilon_D. \qquad (49b)$$

We have normalized the core strengths by $\bar{\rho}\sigma_Y$ so that a core made from the same material as the face-sheets has a non-dimensional strength $0 \le (\bar{\sigma}_l, \bar{\sigma}_t) \le 1$. Note that $\bar{\sigma}_l = 1$ and $\bar{\sigma}_t = 1$ corresponds to a core that achieves the Voigt upper bound on strength in both the transverse and longitudinal directions and this type of core was referred to as the ideal core by Fleck and Deshpande (2004). Following Xue and Hutchinson (2004), the non-dimensional impulse is defined by

$$\bar{I} \equiv \frac{I}{M}\sqrt{\frac{\rho_f}{\sigma_Y}}, \qquad (50)$$

where $M \equiv \left(2\bar{h} + \bar{\rho}\right)\bar{c}\rho_f L$ is the mass per unit area of the sandwich beam. All the above non-dimensional groups are independent groups associated with the sandwich beam geometry, material properties and loading.

In addition we define some dependent non-dimensional groups that are outputs of the model. These are the core compressive strains at the supports and mid-span ε_s and ε_m, respectively, and the time-scales

$$\bar{T} \equiv \frac{T}{\tau},\ \bar{t}_{bd} \equiv \frac{t_{bd}}{\tau},\ \bar{t}_{bs} \equiv \frac{t_{bs}}{\tau} \text{ and } \bar{t}_{eq} \equiv \frac{t_{eq}}{\tau}\ , \qquad (52)$$

where $\tau \equiv L\sqrt{\rho_f / \sigma_Y}$ is the response time of a plastic string of length $2L$ made from a material of yield strength σ_Y and density ρ_f. The non-dimensional mid-span back face deflection and velocity are defined by

$$\bar{w}_b(\bar{t}) \equiv \frac{w_b}{L} \text{ and } \bar{v}_b(\bar{t}) \equiv \frac{v_b \rho_f h_f}{I}, \qquad (53a)$$

respectively, in terms of the non-dimensional time $\bar{t} \equiv t/\tau$. The velocity in Eq. (53a) has been normalized by the representative front face velocity $I/(\rho_f h_f)$ due to the impulse I. This velocity is not equal to the initial velocity v_o of the front face in the lumped mass model because half the core mass is included in the face-sheet mass for the lumped mass model. Similarly, the non-dimensional front face velocity is

$$\bar{v}_f(\bar{t}) \equiv \frac{v_f \rho_f h_f}{I}. \qquad (53b)$$

The dimensionless support reaction is defined by

$$\bar{R}(\bar{t}) = \frac{R\tau}{IL}, \qquad (54)$$

so that $\bar{R} = 1$ corresponds to a temporally uniform reaction force capable of arresting the sandwich beam in time τ. Finally, the non-dimensional maximum back and front face deflections at mid-span are

$$\bar{W}_b \equiv \frac{W_b}{L} \text{ and } \bar{W}_f \equiv \bar{W}_b + \varepsilon_m \bar{c}\ , \qquad (55)$$

respectively.

2.6 Maps showing regimes of behaviour

We proceed to present maps of the regimes of the behaviour in terms of the above non-dimensional groups. The main aim here is to examine the sensitivity of impulse response to the transverse core strength $\bar{\sigma}_t$, the beam aspect ratio $\bar{c}$ and the impulse $\bar{I}$. Maps are plotted with these variables as axes, for the following reference values of properties. The sandwich beams have identical front and back

faces ($\hat{h}=1$) with a face-sheet to core thickness ratio $\bar{h}=0.1$. A core of relative density $\bar{\rho}=0.02$ is assumed to have a nominal densification strain $\varepsilon_D=0.85$ and, consistent with most prismatic core topologies such as the corrugated or diamond core (Cote et al., 2006), the longitudinal strength is assumed to equal the ideal value of $\bar{\sigma}_l=1$.

The regime map with axes $\bar{c}$ and $\bar{\sigma}_t$ is plotted in Fig. 7a for an impulse $\bar{I}=0.09$. Regime B (involving full core densification) dominates the map and, in fact, full core densification occurs at the supports for $\bar{\sigma}_t<0.07$ irrespective of the beam aspect ratio. Regime C occurs at intermediate values of the core strength $\bar{\sigma}_t$. The regime expands with increasing $\bar{c}$, consistent with the expectation that coupling between the core compression and bending phases increases with decreasing length of the sandwich beam. Note that for high values of $\bar{c}$ and $\sigma_t<\sigma_Y h_b^2/L^2$ (case III) there exists a regime where only partial densification of the core occurs giving no back face deflection. This is a decoupled regime and is marked as regime A in Fig. 7a. Contours of normalized core compression time $\bar{t}_{eq}$ are included in Fig. 7a and the boundary between regimes A and C corresponds to $\bar{t}_{eq}\approx 1$. The effect of the impulse value $\bar{I}$ on the regime boundaries is illustrated in Figs. 7b and 7c. With increasing $\bar{I}$, regimes B and D expand at the expense of regimes A and C. Note that the coupled regime with partial core densification (regime C) occurs only over a limited range of $\bar{\sigma}_t$ and $\bar{c}$ values, and the values of $\bar{\sigma}_t$ and $\bar{c}$ for regime C increase with increasing $\bar{I}$.

The effect of impulse magnitude on the regimes of dominance is illustrated in maps with axes $\bar{I}$ and $\bar{\sigma}_t$, as shown in Fig. 8. Consider first the choice $\bar{c}=0.3$, in Fig. 8a: regime B dominates the map. It is evident that we transition from regime A to C to D and then B with increasing $\bar{I}$ for any fixed $\bar{\sigma}_t>0.3$ (i.e in cases I and II). This results from that fact that for small $\bar{I}$, the front and back face velocities equalize very rapidly giving a decoupled response with only partial core densification. An increase in the impulse delays the equalization of front and back face velocities. Yet, back face deceleration time t_{bd} is unchanged and this leads to a coupled response. Further increases in the impulse result in *early* full densification of the core at the supports again giving a decoupled response. The effect of the sandwich beam aspect ratio $\bar{c}$ on the regime boundaries is illustrated in Fig. 8b for the choices $\bar{c}=0.1$ and 0.5. Consistent with the observations in Fig. 7, the decoupled regimes (A and B) shrink while the coupled regimes (C and D) expand with increasing $\bar{c}$.

2.7 Illustrative predictions of the model

We now present some representative predictions of the model with an emphasis on the sensitivity of core compression, face-sheet deflection and support reaction to the transverse strength of the core. All

results are presented for a typical sandwich beam of geometry $\bar{c} = 0.3$, $\bar{h} = 0.1$ and identical front and back faces, $\hat{h} = 1$, loaded with an impulse $\bar{I} = 0.09$. The core is assumed to have a relative density $\bar{\rho} = 0.02$, a densification strain $\varepsilon_D = 0.85$ and a longitudinal strength $\bar{\sigma}_l = 1$. The effect of the transverse strength of the core on the sandwich beam response is investigated for $\bar{\sigma}_t$ in the range $0.001 \le \bar{\sigma}_t \le 0.5$.

The time evolution of normalized mid-span back face deflection $\bar{w}_b \equiv w_b / L$ and mid-span core compression $\varepsilon_c(t) = (w_f - w_b)/c$ are plotted in Figs. 9 and 10, respectively, for four selected values of $\bar{\sigma}_t = 0.001$, 0.06, 0.12 and 0.5. These four values of $\bar{\sigma}_t$ have been chosen such that the sandwich beams lie within regimes B, D, C and A, respectively, (as can de deduced from Fig. 7a). The minimum final mid-span deflection is predicted for $\bar{\sigma}_t = 0.5$ (Regime A) while the maximum deflection occurs for $\bar{\sigma}_t = 0.001$ (Regime B). The mid-span core compression is maximum for $\bar{\sigma}_t = 0.001$ (and nearly equal to the densification strain ε_D, indicating that full core densification occurs over the entire beam span in this case) while the level of core compression is a minimum for the sandwich beam with a transverse core strength $\bar{\sigma}_t = 0.5$. Note that the times $\bar{t}_{eq}$ for core compression to end are the highest for the $\bar{\sigma}_t = 0.06$ and 0.12 sandwich beams that lie in the coupled regimes C and D, respectively.

The four regimes of behaviour are contrasted in plots of the mid-span face-sheet velocity versus time, as shown in Fig. 11 for the four selected values of $\bar{\sigma}_t$.

Regime A : Decoupled regime with partial core densification ($\bar{\sigma}_t = 0.5$)

The front face velocity decreases linearly with time while the back face velocity increases linearly with time until the face-sheet velocities equalize at mid-span (Fig. 11a). At this instant, a discontinuity in the velocity of the mid-span is predicted as the model switches to the modal sandwich solution; the sandwich is subsequently brought to rest. A large increase in the support reaction (Fig. 12a) leads to rapid arrest of the beam in the sandwich phase. The discontinuity in velocity at $t = t_{eq}$ and the rapid arrest of the beam are consequences of approximations inherent in the sandwich phase of the model; this will be made explicit subsequently by comparison with the finite element calculations.

Regime B : Decoupled regime with full core densification ($\bar{\sigma}_t = 0.001$)

A weak core is unable to decelerate the front face significantly and provides negligible loading of the back face (Fig. 11b). Densification of the core occurs over the entire sandwich beam span at $t = t_{eq}$ resulting in the sudden jump in mid-span back face velocity at the instant that the sandwich phase

commences. The support reaction is almost zero up to core densification (Fig. 12b) but displays a sudden rise when the sandwich phase of the motion commences. This support reaction continues to increase gradually over the duration of the sandwich phase of the response.

Regime C : Coupled regime with partial core densification ($\overline{\sigma}_t = 0.12$)

The front face velocity decreases linearly with time while the back face velocity varies sinusoidally with time (Fig. 11c). For this choice of parameters, the back face motion halts before the front face has arrested, and no sandwich phase of the response is present. The support reactions are much smaller in this coupled regime with $\overline{R} \approx 0.5$ over the entire duration of the response (Fig. 12c).

Regime D : Coupled regime with full core densification ($\overline{\sigma}_t = 0.06$)

Similar to regime C, the front face velocity decreases linearly with time while the back face velocity varies sinusoidally (Fig. 11d). Shortly after the back face has arrested (with the front face is still in motion), full densification of the core occurs at the supports and the motion of the beam is then arrested by the sandwich phase of motion. The support reaction remains approximately constant up to full densification of the core (Fig. 12d). Similar to the observations for regimes A and B, there is a sudden increase in this support reaction at the onset of the sandwich phase of motion.

3. Finite element study

Selected comparisons between finite element (FE) predictions and analytical predictions of the responses of monolithic and sandwich beams are presented in this section along with a complete FE investigation of the regimes of behaviour discussed above. All computations were performed using the explicit time integration version of the commercially available FE code ABAQUS (version 6.5). The beams were modelled using four noded plane quadrilateral elements with reduced integration (type CPE4R in ABAQUS notation). Numerical damping associated with volumetric straining in ABAQUS Explicit was switched off by setting the bulk viscosity associated with this damping to zero; preliminary calculations revealed that the default viscosity in ABAQUS results in substantial and misleading artificial viscous dissipation due to the large volumetric compression of the core. In all calculations reported in this section, the sandwich beams have face-sheets with thicknesses $h_f = h_b = 0.01$ m and a core of depth $c = 0.1$ m giving $\overline{h} = 0.1$ and $\hat{h} = 1$. Finite element simulations were performed for selected values of the sandwich aspect ratio $\overline{c}$, obtained by varying the half-span

21

of the beam over the range $0.2\,\mathrm{m} \le L \le 1\,\mathrm{m}$. A mesh with square elements of size $c/50$ was employed in all calculations. Mesh sensitivity studies revealed that additional mesh refinements did not improve the accuracy of the calculations appreciably.

3.1 Constitutive description

Unless otherwise specified, the face-sheets of the sandwich beam comprise an isotropic elastic-ideally plastic solid of yield strength σ_Y, yield strain ε_Y and density ρ_f. The Young's modulus is specified by $E_f \equiv \sigma_Y / \varepsilon_Y$ and the face-sheet material has an elastic Poisson's ratio ν_f. The solid yields in accordance with J2 flow theory. The core is treated as a compressible anisotropic viscoplastic continuum as specified below, and the constitutive law has been implemented in ABAQUS Explicit as a user defined material (VUMAT). Assume the orthotropic axes x_i of the core are aligned with the axes of the beam as sketched in Fig. 1, i.e x_1 and x_2 are aligned with the longitudinal and transverse directions, respectively. Introduce the stress and plastic strain matrices in the usual way as

$$\boldsymbol{\sigma} = (\sigma_1, \sigma_2, \sigma_3, \sigma_4, \sigma_5, \sigma_6)^T \equiv (\sigma_{11}, \sigma_{22}, \sigma_{33}, \sigma_{13}, \sigma_{23}, \sigma_{12})^T, \qquad (56a)$$

and

$$\boldsymbol{\varepsilon}^p = (\varepsilon_1^p, \varepsilon_2^p, \varepsilon_3^p, \varepsilon_4^p, \varepsilon_5^p, \varepsilon_6^p)^T \equiv (\varepsilon_{11}^p, \varepsilon_{22}^p, \varepsilon_{33}^p, \varepsilon_{13}^p, \varepsilon_{23}^p, \varepsilon_{12}^p)^T, \qquad (56b)$$

respectively. Assume complete decoupling of material response between the orthogonal material directions and define the plastic strain rate $\dot{\varepsilon}_i^p$ via an overstress relation as

$$\dot{\varepsilon}_i^p = \begin{cases} \left(\dfrac{|\sigma_i| - Y_i(\varepsilon_i^p)}{\eta} \right) & \text{if } |\sigma_i| > Y_i(\varepsilon_i^p) \\ 0 & \text{otherwise,} \end{cases} \qquad (57)$$

where the yield strength $Y_i(\varepsilon_i^p)$ is a function only of the plastic strain ε_i^p. The material viscosity η is taken to be a constant. The total strain rate $\dot{\varepsilon}_i$ is obtained by supplementing the above anisotropic plasticity model with isotropic elasticity such that

$$\dot{\varepsilon}_i = L_{ij}\dot{\sigma}_j + \dot{\varepsilon}_i^p \,\mathrm{sign}(\sigma_i) \qquad \text{(summation over } j\text{)}. \qquad (58a)$$

In the case of isotropic elasticity, the compliance matrix L_{ij} of the core material is specified in terms of the Young's modulus E_c and Poisson's ratio ν_c as

$$\mathbf{L} = \begin{pmatrix} 1/E_c & -\nu_c/E_c & -\nu_c/E_c & 0 & 0 & 0 \\ & 1/E_c & -\nu_c/E_c & 0 & 0 & 0 \\ & & 1/E_c & 0 & 0 & 0 \\ & & & 2(1+\nu_c)/E_c & 0 & 0 \\ & \text{sym} & & & 2(1+\nu_c)/E_c & 0 \\ & & & & & 2(1+\nu_c)/E_c \end{pmatrix}. \qquad (58b)$$

We employ an isotropic elastic response for simplicity; this suffices as the core response of dictated by the plastic branch. The above elastic-plastic constitutive relation is expected to be adequate to model sandwich cores such as the square-honeycomb core or the corrugated core; see for example Xue et al. (2005). Moreover, an anisotropic constitutive law with a decoupled "yield surface" makes for straightforward comparisons between the FE simulations and the analytical model discussed in Section 2.

Numerical values for the sandwich beam constituent materials are as follows. The face-sheets are assumed to be made from an alloy steel with yield strength $\sigma_Y = 200$ MPa, yield strain $\varepsilon_Y = 0.1\%$, elastic Poisson's ratio $\nu_f = 0.3$ and density $\rho_f = 8000\ \mathrm{kgm}^{-3}$. The core is made from the same material as the face-sheets with a relative density $\bar{\rho} = 0.02$ (i.e. a core density $\rho_c = 160\ \mathrm{kgm}^{-3}$). It is assumed that the core has a high longitudinal strength ($Y_1 \equiv \sigma_l$) and a high shear strength ($Y_6 \equiv \tau_c$) given by $Y_1 = Y_6 = \bar{\rho}\sigma_Y$, and strain hardening in these directions is neglected. These properties are appropriate for prismatic cores made from the same material as the sandwich beam face-sheets. The transverse strength Y_2 is assumed to be independent of the plastic strain ε_2^p up to a nominal densification strain ε_D: beyond densification a linear hardening behaviour is assumed with a very large tangent modulus $E_t = 0.1E_f$. The nominal densification strain is fixed at $\varepsilon_D = 0.85$ while the transverse strength $Y_2 \equiv \sigma_t$ is varied in the parametric studies reported subsequently. The core has a Young's modulus $E_c = \bar{\rho}E_f$ and Poisson's ratio $\nu_c = 0.25$; numerical experiments confirmed that the predictions are insensitive to the elastic stiffness of the core. Finally, we note that the viscosity η of the core was chosen such that the shock width (Radford et al., 2005)

$$l = \frac{\eta\varepsilon_D}{\rho_c v_o}, \tag{59}$$

equals $c/10$. Thus, η was varied in accordance with the value of the impulse I applied. This prescription ensures that the shock width is always much less than the core depth yet is larger than the mesh size. Note that large gradients in stress and strain occur over the shock width and thus a mesh size smaller than l is required to resolve these gradients accurately.

3.2 Boundary conditions

Half the beam was analysed with symmetry boundary conditions imposed at mid-span. The back face was fully clamped at the supports, while the motion of the core and front face was constrained along the x_1 direction at the supports. Impulsive loading was imposed by giving a spatially uniform initial velocity $I/(\rho_f h_f)$ to the front face-sheet.

23

3.3 Finite element results and comparison with analytical predictions for each regime

Recall that the definition of the time t_{bd} is not clear from the FE calculations in the decoupled regimes of behaviour. Thus, the regime definitions, Eq. (48), are reinterpreted for the FE calculations as follows:

Regime A: *partial* core densification is completed at the supports *before* the mid-span of the back face begins to decelerate.

Regime B: *full* core densification occurs at the supports *before* the mid-span of the back face begins to decelerate.

Regime C: *partial* core densification is completed of the core at the supports *after* the mid-span of the back face begins to decelerate.

Regime D: *full* core densification occurs at the supports *after* the mid-span of the back face begins to decelerate.

FE simulations employed the sandwich beam geometry specified in Section 2.7 ($\bar{c} = 0.3$, $\bar{h} = 0.1$ and $\hat{h} = 1$). The FE predictions of the mid-span back face deflection versus time histories and the mid-span core compression versus time histories are included in Figs. 9 and 10, respectively, while the predictions of the final deformed profiles are shown in Fig. 13. While the FE and analytical predictions of the core compression are in good agreement the analytical predictions for the final deflections of the back face of the sandwich beam in regime A ($\bar{\sigma}_t = 0.5$) are substantially lower than the FE predictions. This under-prediction can be tracked back to the fact that the analytical model neglects shear deformation of the core. Both the FE and analytical models predict that the $\bar{\sigma}_t = 0.5$ sandwich beam undergoes negligible core compression and thus the aspect ratio of the sandwich beam remains at $\bar{c} \approx 0.3$ during the subsequent sandwich phase. However, the analytical model neglects shear deformations of the core during the sandwich phase of the motion. These shear deformations are significant for beams with large values of $\bar{c}$ and thus the analytical model under-predicts the deflections of the $\bar{\sigma}_t = 0.5$ sandwich beam.

The FE predictions of the mid-span velocity and support reaction versus time histories are included in Figs. 11 and 12, respectively. We now compare these FE predictions with the analytical estimates for each of the four regimes.

Regime A : Decoupled regime with partial core densification ($\bar{\sigma}_t = 0.5$)

The analytical and FE predictions of the velocity histories (Fig. 11a) are in good agreement up to the end of core compression. Subsequently, the FE calculation gives no velocity discontinuity and a longer

arrest time than the analytical predictions. The reasons for these two discrepancies have already been discussed: (i) the analytical model assumes a sudden switch to the modal solution following the end of core compression and this results in the velocity discontinuity; and (ii) the analytical model neglects shear deformations of the core and consequently predicts the rapid arrest of the sandwich beam after the end of core compression. Consistent with the above, FE and analytical predictions of the support reactions (Fig. 12a) are in good agreement up to the end of core compression. Subsequently, the analytical model grossly over-predicts the support reactions as it overestimates the shear strength of the stubby sandwich beam.

Regime B : Decoupled regime with full core densification regime ($\overline{\sigma}_t = 0.001$)

The FE simulations indicate that upon core densification, travelling hinges initiate at the support of the sandwich beam and propagate to the mid-span. After these hinges coalesce at mid-span, the beam arrests by plastic bending and stretching. This travelling hinge phase is neglected in the analytical model and this results in the discrepancy between the analytical and FE predictions of the face-sheet velocity and support reaction histories plotted in Figs. 11b and 12b, respectively. Despite this, the analytical model accurately predicts the final back face deflection and core compression (Figs. 9a and 10).

Regime C : Coupled regime with partial core densification ($\overline{\sigma}_t = 0.12$)

The analytical and FE predictions of the mid-span front and back face velocity versus time histories (Fig. 11c) and of the support reaction versus time histories (Fig. 12c) are in good agreement. In this regime, a sandwich phase of response is predicted by neither the analytical model nor the FE model.

Regime D : Coupled regime with full core densification ($\overline{\sigma}_t = 0.06$)

The FE and analytical predictions of the velocity histories (Fig. 11d) and support reaction (Fig. 12d) are in reasonable agreement up to the full densification of the core. In line with the above discussion, the discrepancies between the two sets of predictions are maximum in the sandwich phase of the analytical model.

It is clear from Figs. 9-13 that the qualitative nature of the response is sensitive to the magnitude of $\overline{\sigma}_t$. For the choice $\bar{I} = 0.09$ and $\bar{c} = 0.3$, as $\overline{\sigma}_t$ increases from 0.001 to 0.12 the regime of response switches through the sequence B, D, C and A. Also, the deflection $\overline{W}_b$ is a minimum for the choice

$\bar{\sigma}_t = 0.06$ according to the FE simulation shown in Fig. 9. It is of interest to determine whether these conclusions change for other values of $\bar{I}$ and $\bar{c}$.

3.4 Effect of core transverse strength upon response over ranges of impulse and core thickness

The analytical and FE predictions of the final mid-span back face deflections are plotted in Fig. 14 as functions of the normalised transverse core strength $\bar{\sigma}_t$. (In the FE calculations the final back face deflection at the mid-span is taken to be the time average of the displacement, after the initial peak deflection, over four cycles of the elastic vibrations.) In Fig. 14a, comparisons are shown for sandwich beams with aspect ratio $\bar{c} = 0.3$ at selected values of the loading impulse $\bar{I}$ while in Fig. 14b the analytical and FE predictions of $\overline{W}_b$ are compared for selected values of $\bar{c}$ at an impulse $\bar{I} = 0.09$. Good agreement between numerical and analytical predictions is observed for $\bar{\sigma}_t < 0.1$ but typically, the analytical model under-predicts the deflections for the high transverse core strength sandwich beams that lie in regime A ($\bar{\sigma}_t > 0.1$). The active regimes for each of the FE simulations, ascertained according to the criteria given at the beginning of Section 3.3, are indicated in Figure 14. The transition with increasing core strength from regimes B → D → C → A is generally observed, though regime C does not arise for the $\bar{I} = 0.18$ case in Fig. 14a and neither regimes C nor D occur for the $\bar{c} = 0.1$ case in Fig. 14b. The deflection $\overline{W}_b$ tends to decrease with increasing $\bar{\sigma}_t$ for regimes A and B; $\overline{W}_b$ increases with increase in $\bar{\sigma}_t$ in regime C.

Comparisons between FE and analytical predictions of $\bar{t}_{eq}$ as a function of $\bar{\sigma}_t$ are presented in Fig. 15a for $\bar{c} = 0.3$ and selected values of the loading impulse $\bar{I}$. Similar comparisons are shown in Fig. 15b for $\bar{I} = 0.09$ and selected values of $\bar{c}$. Taken together, these comparisons demonstrate the accuracy of the analytical model in predicting $\bar{t}_{eq}$ over the full range of $\bar{\sigma}_t$ values considered here. This confirms the observation that the analytical model is accurate prior to the equalisation of the face-sheet velocities but is less accurate in the sandwich phase for the reasons discussed above. We expect the analytical model to predict accurately the boundaries of the regimes of behaviour (see Section 3.5). The regimes marked in Fig. 14 indicate that $\bar{t}_{eq}$ tends to increase with increasing $\bar{\sigma}_t$ for regimes B and D while it typically decreases with increasing $\bar{\sigma}_t$ for regimes A and C. A more comprehensive assessment of performance across the regimes is given in Section 3.6.

3.5 Comparison of sandwich beams with monolithic beams of equal mass

It is of practical interest to determine whether sandwich beams are more blast resistant than monolithic beams of equal mass. Appropriate performance metrics are the maximum back face deflection and the

maximum support reaction for a given blast impulse. We now use the FE methods to make comparisons of the blast resistance for monolithic and sandwich beams of equal mass in order to determine the conditions under which sandwich beams outperform monolithic beams.

The fully-clamped monolithic beams of span $2L$ and thickness H are assumed to be made from the same material as the face-sheets of the sandwich beams. In order for the monolithic beams to have the same areal mass M as that of the sandwich beams, the aspect ratio of the monolithic beams is

$$\frac{H}{L} = (2\bar{h} + \bar{\rho})\bar{c} \,. \qquad (60)$$

Four noded plane quadrilateral elements with reduced integration (CPE4R in the ABAQUS notation) are used to represent the monolithic beams. Square elements of side $H/10$ were used and the beam was loaded by imparting a spatially uniform initial velocity $I/(\rho_f H)$ to the beam. We define the permanent mid-span deflection of the back face of the monolithic beam as W_b^{mon} and the maximum support reaction as $R_{\max}^{mon}$. The corresponding normalised values are $\overline{W}_b^{mon} \equiv W_b^{mon}/L$ and $\overline{R}_{\max}^{mon} \equiv R_{\max}^{mon}\tau/(IL)$. For the sandwich beams, the normalised permanent back face deflection and maximum support reaction are $\overline{W}_b \equiv W_b/L$ and $\overline{R}_{\max} \equiv R_{\max}\tau/(IL)$, respectively.

The relative performance of the sandwich beam to the monolithic beam is quantified by the ratios $\overline{W}_b/\overline{W}_b^{mon}$ and $\overline{R}_{\max}/\overline{R}_{\max}^{mon}$. These are plotted as a function of the transverse core strength $\bar{\sigma}_t$ in Fig. 16 for $\bar{c} = 0.3$ and for selected values of $\bar{I}$. The sandwich beams deflect less than monolithic beams within a narrow range of core strengths $\bar{\sigma}_t$ and the optimal strength increases with increasing $\bar{I}$. At very large $\bar{\sigma}_t$ and very small $\bar{\sigma}_t$, the back face deflections of sandwich beams can exceed those of the monolithic beams. In contrast, over the full range of transverse core strengths considered here, the maximum support reactions of the sandwich beams are lower than those of the monolithic beams. It is encouraging to note that both the back face deflections and support reactions of the sandwich beams are at their minimum at approximately the same value of $\bar{\sigma}_t$; this is in agreement with recent findings of Liang et al. (2006).

The ratios $\overline{W}_b/\overline{W}_b^{mon}$ and $\overline{R}_{\max}/\overline{R}_{\max}^{mon}$ are plotted as a function of the transverse core strength $\bar{\sigma}_t$ in Figs. 17a and 17b, respectively, for selected values of $\bar{c}$ and $\bar{I} = 0.09$. Again we observe that $\overline{W}_b/\overline{W}_b^{mon}$ less than unity over only a narrow range of core strengths $\bar{\sigma}_t$; the ratio $\overline{R}_{\max}/\overline{R}_{\max}^{mon}$ has a minimum value over this same range of $\bar{\sigma}_t$. In contrast to the predictions of Fig. 16b, we observe in Fig. 17b that the maximum support reactions of the $\bar{c} = 0.1$ sandwich beam exceed those of the corresponding monolithic beam for core strengths $\bar{\sigma}_t < 0.05$. The results presented in Figs. 16 and 17

taken together indicate that appropriately designed sandwich beams outperform monolithic beams of equal mass but due care must be taken in designing such sandwich beams to resist blast loading. The benefit of sandwich construction over monolithic loading is limited to a finite range of $\bar{I}$. The active regimes for each of the FE simulations are again indicated. In Figs. 16a and 17a, the support reactions are observed to decrease with increasing $\bar{\sigma}_t$ for Regimes B and D and to increase with increasing $\bar{\sigma}_t$ for Regimes A and C.

3.6 Optimal performance of the sandwich beams

The results of Section 3.5 indicate that there exists a narrow range of transverse core strength over which the sandwich beams have their optimal performance in terms of minimizing the back face deflection or support reaction. We can envisage two typical design situations for the design of blast resistant sandwich beams:

(i) For a given blast impulse, determine the optimal value of $\bar{\sigma}_t$ as a function of the sandwich beam aspect ratio $\bar{c}$.

(ii) For a given sandwich beam aspect ratio $\bar{c}$, determine the optimal value of $\bar{\sigma}_t$ as a function of the blast impulse $\bar{I}$.

Here we determine these optimal strengths to minimize either the back face deflections or support reactions.

Figure 18a shows a design chart with axes $\bar{c}$ and $\bar{\sigma}_t$ for sandwich beams subject to an impulse $\bar{I} = 0.09$. FE (dashed lines) and analytical (thick solid lines) predictions of the regime boundaries are marked on the map.

The FE and analytical predictions of the regime boundaries are in good agreement (Fig. 18a) except for the boundary between regimes B and D. The boundary between regimes B and D is largely co-incident with the case II-case III boundary in the analytical calculations (see Fig. 18a) as a result of the fact that the analytical calculations predict no back face deflection for $\sigma_t < \sigma_Y h_b^2 / L^2$ prior to the end of core compression. On the other hand, in the FE calculations some back face deflection always occurs due to the finite elastic modulus of the face-sheet material in these calculations and thus we do not expect the FE and analytical predictions of the regime boundaries in this domain to be in good agreement.

Contours of the FE predictions of the non-dimensional maximum mid-span back face deflection $\overline{W}_b$ are included in Fig. 18a for the purposes of selecting the core strengths that minimise the back face deflections for a given value of $\bar{c}$. The trajectory of arrows in Fig. 18a traces the optimum designs (i.e.

core strengths $\overline{\sigma}_t$ that minimize $\overline{W}_b$ for a given $\overline{c}$) with increasing $\overline{c}$. Note that the optimum designs lie in the regimes in which full densification of the core occurs at the supports (i.e. in regimes B and D) and the optimum values of $\overline{\sigma}_t$ increases with increasing $\overline{c}$. An alternative objective might be to minimise the support reactions. For the purposes of performing this optimisation we plot in Fig. 18b, FE predictions of the contours of the normalised maximum support reaction $\overline{R}_{\max} \equiv R_{\max}\tau/(IL)$ on a map with axes $\overline{c}$ and $\overline{\sigma}_t$. The trajectory of arrows traces the path of optimum designs (i.e. core strengths $\overline{\sigma}_t$ that minimize $\overline{R}_{\max}$ for a given $\overline{c}$) with increasing $\overline{c}$. The path indicates that the optimum value of $\overline{\sigma}_t$ is approximately the same for all values of $\overline{c}$ considered here. Note that these optimum designs do not lie in the regimes where full densification occurs and in fact there is a sharp rise in the support reaction near the boundary between partial densification and full densification. A comparison of the optimum designs from Figs. 18a and 18b indicates that the value of $\overline{\sigma}_t$ required to minimise $\overline{W}_b$ is less than that required to minimise $\overline{R}_{\max}$.

We next consider the design problem of determining the optimum core strength $\overline{\sigma}_t$ as a function of the blast impulse $\bar{I}$ for sandwich beams with $\overline{c} = 0.3$. A design chart with axes $\bar{I}$ and $\overline{\sigma}_t$ is plotted in Fig. 19a. The FE (dashed lines) and analytical (thick solid lines) predictions of the regime boundaries marked in Fig. 19a are in good agreement (expect for boundaries betweens regimes B and D for the reasons discussed above), indicating that the analytical model suffices to predict the regimes of behaviour. Contours of the FE predictions of $\overline{W}_b$ are included in Fig. 19a along with arrows tracing the optimum path (i.e. core strengths $\overline{\sigma}_t$ that minimize $\overline{W}_b$ for a given $\bar{I}$) with increasing $\bar{I}$. The optimum designs lie approximately near the boundary between regimes C and D. Contours of $\overline{R}_{\max}$ (for $\overline{c} = 0.3$) are marked in the map in Fig. 19b along with arrows tracing the optimum path (i.e. core strengths $\overline{\sigma}_t$ that minimize $\overline{R}_{\max}$ for a given $\bar{I}$) with increasing $\bar{I}$. Note that the value of $\overline{\sigma}_t$ which minimises $\overline{W}_b$ for a given value of $\bar{I}$ also minimises $\overline{R}_{\max}$. But the best value of $\overline{\sigma}_t$ increases with increasing $\bar{I}$. Consequently, a sandwich beam designed to be optimal for a given blast impulse is suboptimal for other blast loadings. We expect that the specification of core strength involves additional considerations such as constraints on the allowable core compression so that the sandwich beam retains some level of structural integrity after the blast event.

4. Limitations of the analysis

The analytical and FE calculations presented herein elucidate the regimes of behaviour of sandwich beams subject to impulsive loading. The results presented here are largely consistent with the recent full three-dimensional FE simulations of Liang et al. (2006) and McShane et al. (2006). Both these

previous studies had shown possible performance enhancements for sandwich beams with low transverse strength cores. However, in order to be comparable with an analytical model, the current study has made a number of additional simplifying assumptions compared with those of Liang et al. (2006) and McShane et al. (2006), and the consequences of these simplifications are now addressed.

(a) In the current study, the problem under consideration was simplified by neglecting the effects of fluid-structure interaction. Typically, a much smaller fraction of the blast impulse is transmitted into a sandwich beam (at least from an underwater explosion) compared to that transmitted into a monolithic beam of equal mass, see for example Fleck and Deshpande (2004). Thus, in the underwater blast loading investigations of Liang at al. (2006) and McShane et al. (2006), sandwich beams always outperform monolithic beams of equal mass. On the other hand, we show here that monolithic beams (subject to the same blast impulse as sandwich beams) can outperform inadequately designed sandwich beams; see Figs. 16 and 17. The results from the present study will need to be modified to include the effects of fluid-structure interaction in order to fully demonstrate the performance enhancements that can be achieved by employing sandwich construction. Note that to a first approximation, the underwater blast performance of the sandwich beams can be estimated by correcting the impulse $\bar{I}$ in the manner suggested by Deshpande and Fleck (2005) or Hutchinson and Xue (2005).

(b) We employ a homogenised foam-like core constitutive relation. Such a relation is adequate for foam cores and is also expected to suffice for stacked cores such as the diamond lattice core (Cote et al., 2006). However, it is unclear whether such a constitutive description is adequate for the corrugated, I-frame and Y-frame prismatic cores investigated by Liang et al. (2006) and McShane et al. (2006). We employed the foam-like constitutive description here in order to ensure that the core has a well-defined strength. This enabled us to make direct comparisons with the analytical models and provide some insight into the effect of core strength on the sandwich beam performance.

(c) We note that Liang et al. (2006) and McShane et al. (2006) modelled sandwich beams made from stainless steel. Thus, they modelled the face-sheets as solids with a strong strain hardening characteristic while here we modelled the face-sheets as ideally-plastic solids. The main aim of the present investigation was to elucidate the regimes of behaviour rather than to investigate the blast response of specific sandwich structures.

5. Concluding remarks

The impulsive response of sandwich beams has been analysed by an analytical lumped mass model and by finite element simulations. The analytical model is able to estimate the deflections, core compression and support reactions of the sandwich beams. It suggests four distinct regimes of

sandwich beam behaviour by comparing the time-scale of the back face response with the time required to equalise the front and back face velocities. Maps showing the dominance of the four regimes are constructed to illustrate the effect of the sandwich beam aspect ratio $\bar{c}$, transverse core strength $\bar{\sigma}_t$ and blast impulse $\bar{I}$ on the type of response. Typically, for a given impulse $\bar{I}$, there is coupling between the core compression and the combined beam bending and stretching stages of sandwich beam response at intermediate values of the transverse core strength and at high values of $\bar{c}$. Increasing the level of impulse increases the dominance of the regimes in which full densification of the core occurs.

Finite element (FE) calculations of the impulse response of the sandwich beams are reported over a wide range of values of $\bar{c}$, $\bar{\sigma}_t$ and blast impulse $\bar{I}$. A comparison between the FE and analytical predictions indicates that the analytical model captures the response of the sandwich beam to a high level of accuracy up to the end of core compression. Consequently, the analytical model accurately predicts the regimes of behaviour of the sandwich beam. However, the analytical model neglects the effect of travelling hinges after the end of core compression. It under-predicts the deflections and over-predicts support reactions during the sandwich phase of motion in which the front and back faces share a common velocity. Sandwich beams with a high core strength undergo a significant fraction of their deflection in this phase and thus the model is least accurate for such beams. Encouragingly, the predictions of the optimal cores strengths from the analytical and FE calculations are in good agreement.

The FE calculations indicate that appropriately designed sandwich beams can undergo significantly smaller deflections and exert smaller forces on the supports compared to monolithic beams of equal mass subject to the same blast impulse. It is recognised that sandwich beams show additional benefit over monolithic beams due to the reduced transmitted impulse as a consequence of fluid-structure interaction. Design charts are constructed to select the optimal transverse core strength that either minimise the back face deflections or support reactions for a given $\bar{I}$ or $\bar{c}$. Values of $\bar{\sigma}_t$ that minimize the back face deflections also typically minimise the support reactions. However, these values increase with increasing blast impulse and thus a sandwich beam designed to be optimal for a given blast impulse is suboptimal for other blast loadings.

Acknowledgements

The authors are grateful to ONR for their financial support through US-ONR IFO grant number N00014-03-1-0283 on The Science and Design of Blast Resistant Sandwich Structures.

References

Côté, F., Deshpande, V. S., Fleck, N. A. and Evans, A. G. (2006). The compressive and shear responses of corrugated and diamond lattice materials, *International Journal of Solids and Structures*, in press.

Deshpande, V. S. and Fleck, N. A. (2005). A. One-dimensional response of sandwich plates to underwater shock loading, *Journal of the Mechanics and Physics of Solids*, 53(11): 2347-2383.

Fleck, N. A. and Deshpande, V. S. (2004). The resistance of clamped sandwich beams to shock loading, *Journal of Applied Mechanics*, 71(3): 386-401.

Hutchinson, J. W. and Xue, Z. (2005). Metal sandwich plates optimised for pressure pulses, *International Journal of Mechanical Sciences,* 47(4-5): 545-569.

Jones, N. (1989). *Structural Impact*, Cambridge, UK: Cambridge University Press

Liang, Y., Spuskanyuk, A. V., Flores, S. E., Hayhurst, D. R., Hutchinson, J. W., McMeeking, R. M. and Evans, A. G. (2006) The response of metallic sandwich panels of water blast, to appear in *Journal of Applied Mechanics.*

McShane, G. J., Deshpande, V. S. and Fleck, N. A. (2006). The underwater blast resistance of metallic sandwich beams with prismatic lattice cores, to appear in *Journal of Applied Mechanics.*

Rabczuk, T., Kim, J. Y., Samaniego, E. and Belytschko, T. (2004). Homogenization of sandwich structures, *International Journal for Numerical Methods in Engineering,* 61(7): 1009-1027.

Radford, D. D., Deshpande, V. S. and Fleck, N. A. (2005). The use of metal foam projectiles to simulate shock loading on a structure, *International Journal of Impact Engineering*, 31(9):1152-1171.

Taylor, G. I. (1941). *The scientific papers of G I Taylor, Vol III*, Cambridge University Press, 1963, The pressure and impulse of submarine explosion waves on plates, pp. 287-303.

Xue, Z. and Hutchinson, J. W. (2004). A comparative study of blast-resistant metal sandwich plates, *International Journal of Impact Engineering* 30(10): 1283-1305.

Xue, Z., Vaziri, A., and Hutchinson, J. W. (2005). Non-uniform hardening constitutive model for compressible orthotropic materials with application to sandwich plate cores, *Computer Modeling and Simulation in Engineering* 10(1): 79-96.

List of Figures

Figure 1: Geometry of the sandwich beam and schematic of the problem under consideration.

Figure 2: Velocity versus time histories of the mid-span of the front and back faces for three types of sandwich response: (a) "strong core", (b) "slapping" occurs for full core densification at supports before velocity equalisation and (c) "soft core" type sandwich response, as identified by Liang *et al*. (2006).

Figure 3: A sketch summarising the model of the sandwich beam subject to impulse loading. In this lumped mass model, the front face is decelerated by the core while the back face is loaded by the core.

Figure 4: Analysis of the response of the back face: (a) Velocity profile in phase I, (b) free-body diagram of the half-beam in phase I with the deflected shape sketched approximately, (c) velocity profile in phase II, and (d) a free-body diagram of the half-beam in phase II, with the deflected shape sketched approximately. Accelerations are included in (b) and (d).

Figure 5: Analysis of the response of the sandwich beam after the end of core compression. (a) The position of the plastic neutral axis in the undeformed sandwich beam. (b) The configuration of the sandwich beam at $t = t_{eq}$ and (c) a free-body diagram for the half sandwich beam for $t > t_{eq}$. The velocity and acceleration of the plastic neutral axis vary linearly with position.

Figure 6: The four regimes of behaviour determined by comparing time-scales in the response of the sandwich beam. Sketches of typical velocity profiles in each regime of behaviour illustrate the differences between the regimes.

Figure 7: Maps of the regimes of behaviour of the sandwich beam with axes $\bar{c}$ and $\bar{\sigma}_t$. In these maps the beam geometrical parameters are $\bar{h} = 0.1$ and $\hat{h} = 1$ while the fixed core properties are $\bar{\rho} = 0.02$, $\varepsilon_D = 0.85$ and $\bar{\sigma}_l = 1$. (a) Map for an impulse $\bar{I} = 0.09$ with contours of $\bar{t}_{eq}$ included. The effect of the impulse $\bar{I}$ on the regime boundaries for (b) $\bar{I} = 0.045$ and (c) $\bar{I} = 0.135$.

Figure 8: Maps of the regimes of behaviour of the sandwich beam with axes $\bar{I}$ and $\bar{\sigma}_t$. In these maps the beam geometrical parameters are $\bar{h} = 0.1$ and $\hat{h} = 1$ while the fixed core properties are $\bar{\rho} = 0.02$,

33

$\varepsilon_D = 0.85$ and $\overline{\sigma}_l = 1$. (a) Map for a sandwich beam with $\overline{c} = 0.3$ including contours of $\overline{t}_{eq}$. The effect of the sandwich beam aspect ratio on the regime boundaries for (b) $\overline{c} = 0.1$ and (c) $\overline{c} = 0.5$.

Figure 9: Analytical and FE predictions of the normalised mid-span back face deflection $\overline{w}_b$ versus time histories for sandwich beams in (a) the decoupled regimes A and B and (b) in the coupled regimes C and D. Results are shown for sandwich beams with $\overline{c} = 0.3$ subject to an impulse $\overline{I} = 0.09$ and representative values of core strength $\overline{\sigma}_t$ for each regime, as labelled. All other properties of the sandwich beam are fixed at the reference values, i.e. beam geometry $\overline{h} = 0.1$, $\hat{h} = 1$ and core properties $\overline{\rho} = 0.02$, $\varepsilon_D = 0.85$ and $\sigma_l = \tau_c = \overline{\rho}\sigma_Y$.

Figure 10: Analytical and FE predictions of the mid-span core compression ε_c versus time histories. Results are shown for sandwich beams with $\overline{c} = 0.3$ subject to an impulse $\overline{I} = 0.09$ and representative values of core strength $\overline{\sigma}_t$ for each regime, as labelled. All other properties of the sandwich beam are fixed at the reference values, i.e. beam geometry $\overline{h} = 0.1$, $\hat{h} = 1$ and core properties $\overline{\rho} = 0.02$, $\varepsilon_D = 0.85$ and $\sigma_l = \tau_c = \overline{\rho}\sigma_Y$.

Figure 11: Analytical and FE predictions of the normalised mid-span front and back face-sheet velocity versus time histories for sandwich beams with $\overline{c} = 0.3$ subject to an impulse $\overline{I} = 0.09$. All other properties of the sandwich beam are fixed at the reference values, i.e. beam geometry $\overline{h} = 0.1$, $\hat{h} = 1$ and core properties $\overline{\rho} = 0.02$, $\varepsilon_D = 0.85$ and $\sigma_l = \tau_c = \overline{\rho}\sigma_Y$. (a) Regime A with $\overline{\sigma}_t = 0.5$, (b) regime B with $\overline{\sigma}_t = 0.001$, (c) regime C with $\overline{\sigma}_t = 0.12$ and (d) regime D with $\overline{\sigma}_t = 0.06$.

Figure 12: Analytical and FE predictions of the normalised support reaction versus time histories. for $\overline{c} = 0.3$ sandwich beams subject to an impulse $\overline{I} = 0.09$. All other properties of the sandwich beam are fixed at the reference values, i.e. beam geometry $\overline{h} = 0.1$, $\hat{h} = 1$ and core properties $\overline{\rho} = 0.02$, $\varepsilon_D = 0.85$ and $\sigma_l = \tau_c = \overline{\rho}\sigma_Y$. (a) Regime A with $\overline{\sigma}_t = 0.5$, (b) regime B with $\overline{\sigma}_t = 0.001$, (c) regime C with $\overline{\sigma}_t = 0.12$ and (d) regime D with $\overline{\sigma}_t = 0.06$.

Figure 13: Finite element predictions of the (a) initial and (b-e) final deformed profiles of sandwich beams with $\overline{c} = 0.3$ subject to an impulse $\overline{I} = 0.09$. (b) Regime A with $\overline{\sigma}_t = 0.5$, (c) regime B with $\overline{\sigma}_t = 0.001$, (d) regime C with $\overline{\sigma}_t = 0.12$ and (e) regime D with $\overline{\sigma}_t = 0.06$. All other properties of the sandwich beam are fixed at the reference values, i.e. beam geometry $\overline{h} = 0.1$, $\hat{h} = 1$ and core properties $\overline{\rho} = 0.02$, $\varepsilon_D = 0.85$ and $\sigma_l = \tau_c = \overline{\rho}\sigma_Y$.

34

Figure 14: Comparison between analytical and FE predictions of the normalised permanent mid-span back face deflections for a range of transverse core strengths $\bar{\sigma}_t$. (a) Sandwich beams with $\bar{c} = 0.3$ for four selected values of the impulse $\bar{I}$. (b) Sandwich beams subject to an impulse $\bar{I} = 0.09$ for three selected values of $\bar{c}$. All other properties of the sandwich beam are fixed at the reference values, i.e. beam geometry $\bar{h} = 0.1$, $\hat{h} = 1$ and core properties $\bar{\rho} = 0.02$, $\varepsilon_D = 0.85$ and $\sigma_l = \tau_c = \bar{\rho}\sigma_Y$.

Figure 15: Comparison between analytical and FE predictions of the normalised core compression duration $\bar{t}_{eq}$ for a range of transverse core strengths $\bar{\sigma}_t$. (a) Sandwich beams with $\bar{c} = 0.3$ for three selected values of the impulse $\bar{I}$. (b) Sandwich beams subject to an impulse $\bar{I} = 0.09$ for three selected values of $\bar{c}$. All other properties of the sandwich beam are fixed at the reference values, i.e. beam geometry $\bar{h} = 0.1$, $\hat{h} = 1$ and core properties $\bar{\rho} = 0.02$, $\varepsilon_D = 0.85$ and $\sigma_l = \tau_c = \bar{\rho}\sigma_Y$.

Figure 16: Finite element predictions comparing the performance of sandwich beams with $\bar{c} = 0.3$ and monolithic beams of equal mass. (a) The permanent mid-span back face deflections and (b) peak support reactions forces of sandwich beams normalised by that of monolithic beams of equal mass for four selected values of the impulse $\bar{I}$. Predictions are shown for a range of transverse core strengths $\bar{\sigma}_t$. All other properties of the sandwich beam are fixed at the reference values, i.e. beam geometry $\bar{h} = 0.1$, $\hat{h} = 1$ and core properties $\bar{\rho} = 0.02$, $\varepsilon_D = 0.85$ and $\sigma_l = \tau_c = \bar{\rho}\sigma_Y$.

Figure 17: Finite element predictions comparing the performance of sandwich beams with monolithic beams of equal mass subject to an impulse $\bar{I} = 0.09$. (a) The peak mid-span back face deflections and (b) peak support reactions forces of sandwich beams normalised by that of monolithic beams of equal mass for three selected values of the sandwich beam slenderness ratio $\bar{c}$. Predictions are shown for a range of transverse core strengths $\bar{\sigma}_t$. All other properties of the sandwich beam are fixed at the reference values, i.e. beam geometry $\bar{h} = 0.1$, $\hat{h} = 1$ and core properties $\bar{\rho} = 0.02$, $\varepsilon_D = 0.85$ and $\sigma_l = \tau_c = \bar{\rho}\sigma_Y$.

Figure 18: Design charts for sandwich beams with axes $\bar{c}$ and $\bar{\sigma}_t$ constructed for a blast impulse $\bar{I} = 0.09$. (a) FE predictions of the contours of the normalised permanent mid-span back face deflections $\bar{W}_b$. The FE (dashed lines) and analytical (thick solid lines) predictions of the regime boundaries are included. (b) FE predictions of the contours of the normalised peak support reaction force $\bar{R}_{\max}$. In these charts the fixed beam geometrical parameters are $\bar{h} = 0.1$ and $\hat{h} = 1$ while the fixed core properties are $\bar{\rho} = 0.02$, $\varepsilon_D = 0.85$ and $\sigma_l = \tau_c = \bar{\rho}\sigma_Y$. The arrows in (a) and (b) trace the path of designs that minimize $\bar{W}_b$ and $\bar{R}_{\max}$ respectively, for a given $\bar{c}$.

35

Figure 19: Design charts for $\bar{c} = 0.3$ sandwich beams with axes $\bar{I}$ and $\bar{\sigma}_t$. (a) FE predictions of the contours of the normalised permanent mid-span back face deflections $\overline{W}_b$. The FE (dashed lines) and analytical (thick solid lines) predictions of the regime boundaries are also included. (b) FE predictions of the contours of the normalised peak support reaction force $\overline{R}_{\max}$. In these charts the fixed beam geometrical parameters are $\bar{h} = 0.1$ and $\hat{h} = 1$ while the fixed core properties are $\bar{\rho} = 0.02$, $\varepsilon_D = 0.85$ and $\sigma_l = \tau_c = \bar{\rho}\sigma_Y$. The arrows in (a) and (b) trace the path of designs that minimize $\overline{W}_b$ and $\overline{R}_{\max}$ respectively, for a given $\bar{I}$.

36

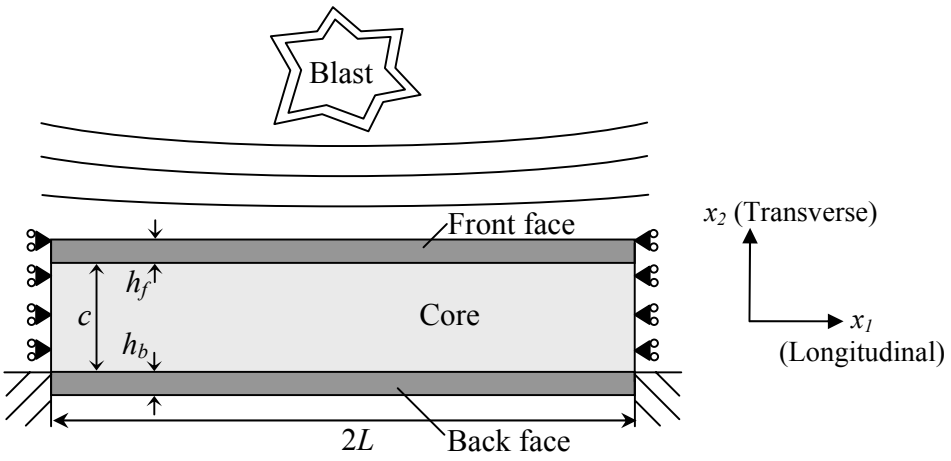

Figure 1: Geometry of the sandwich beam and schematic of the problem under consideration.

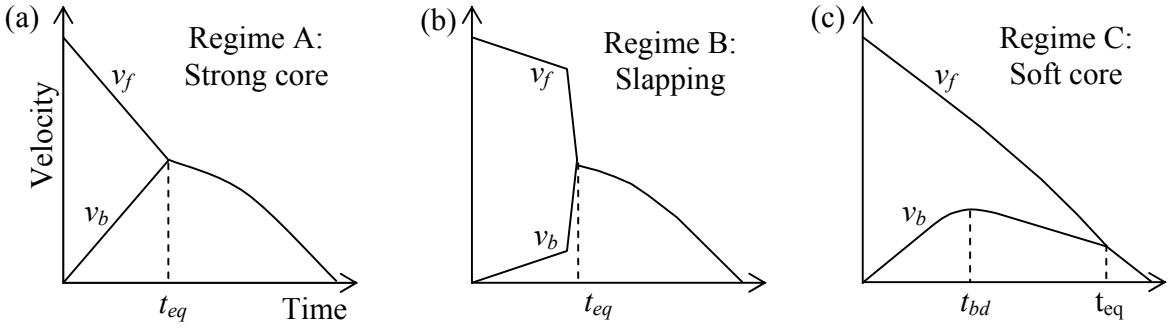

Figure 2: Velocity versus time histories of the mid-span of the front and back faces for three types of sandwich response: (a) "strong core", (b) "slapping" occurs for full core densification at supports before velocity equalisation and (c) "soft core" type sandwich response, as identified by Liang *et al*. (2006).

37

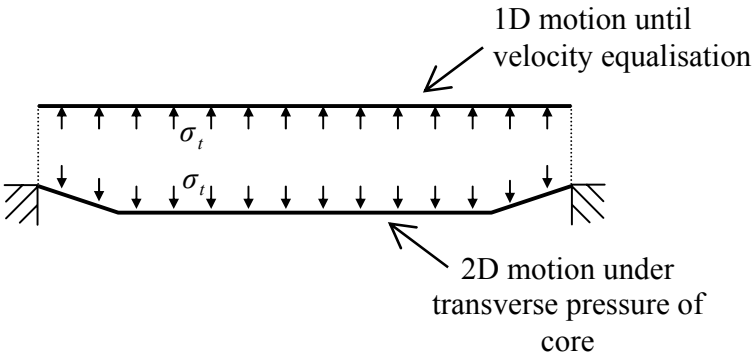

Figure 3: A sketch summarising the model of the sandwich beam subject to impulse loading. In this lumped mass model, the front face is decelerated by the core while the back face is loaded by the core.

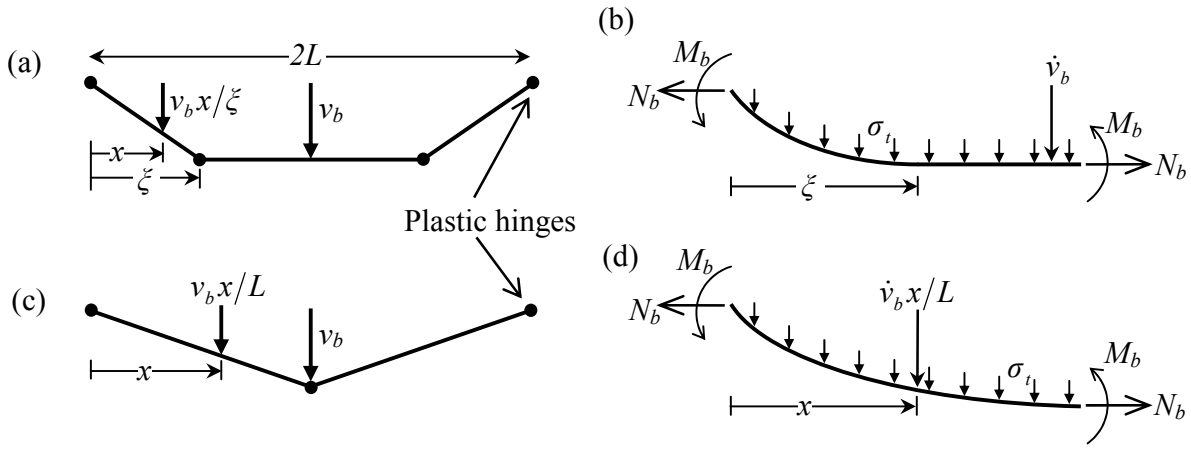

Figure 4: Analysis of the response of the back face: (a) Velocity profile in phase I, (b) free-body diagram of the half-beam in phase I with the deflected shape sketched approximately, (c) velocity profile in phase II, and (d) a free-body diagram of the half-beam in phase II, with the deflected shape sketched approximately. Accelerations are included in (b) and (d).

38

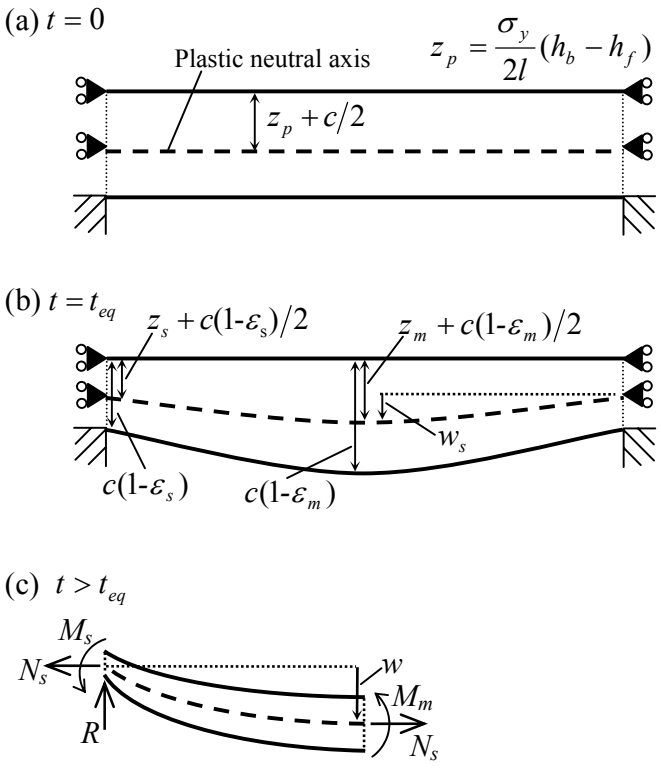

Figure 5: Analysis of the response of the sandwich beam after the end of core compression. (a) The position of the plastic neutral axis in the undeformed sandwich beam. (b) The configuration of the sandwich beam at $t = t_{eq}$ and (c) a free-body diagram for the half sandwich beam for $t > t_{eq}$. The velocity and acceleration of the plastic neutral axis vary linearly with position.

39

	Decoupled, $t_{eq} < t_{bd}$	Coupled, $t_{eq} > t_{bd}$
Incomplete core densification, $t_{eq} < t_D$	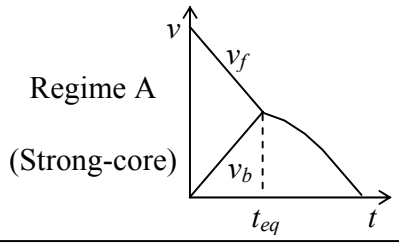	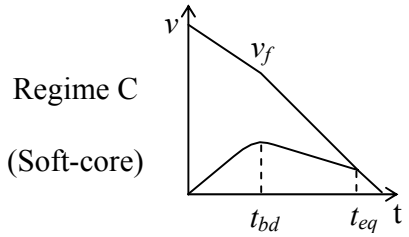
Complete core densification, $t_{eq} = t_D$	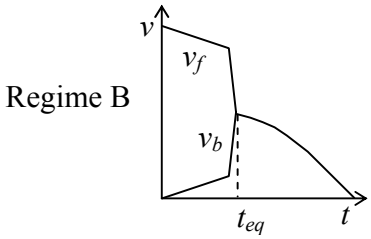	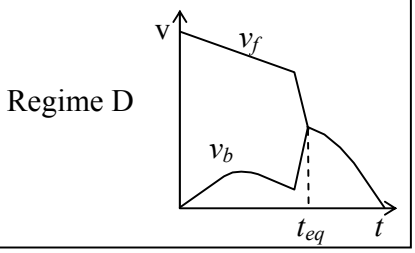

Figure 6: The four regimes of behaviour determined by comparing time-scales in the response of the sandwich beam. Sketches of typical velocity profiles in each regime of behaviour illustrate the differences between the regimes.

40

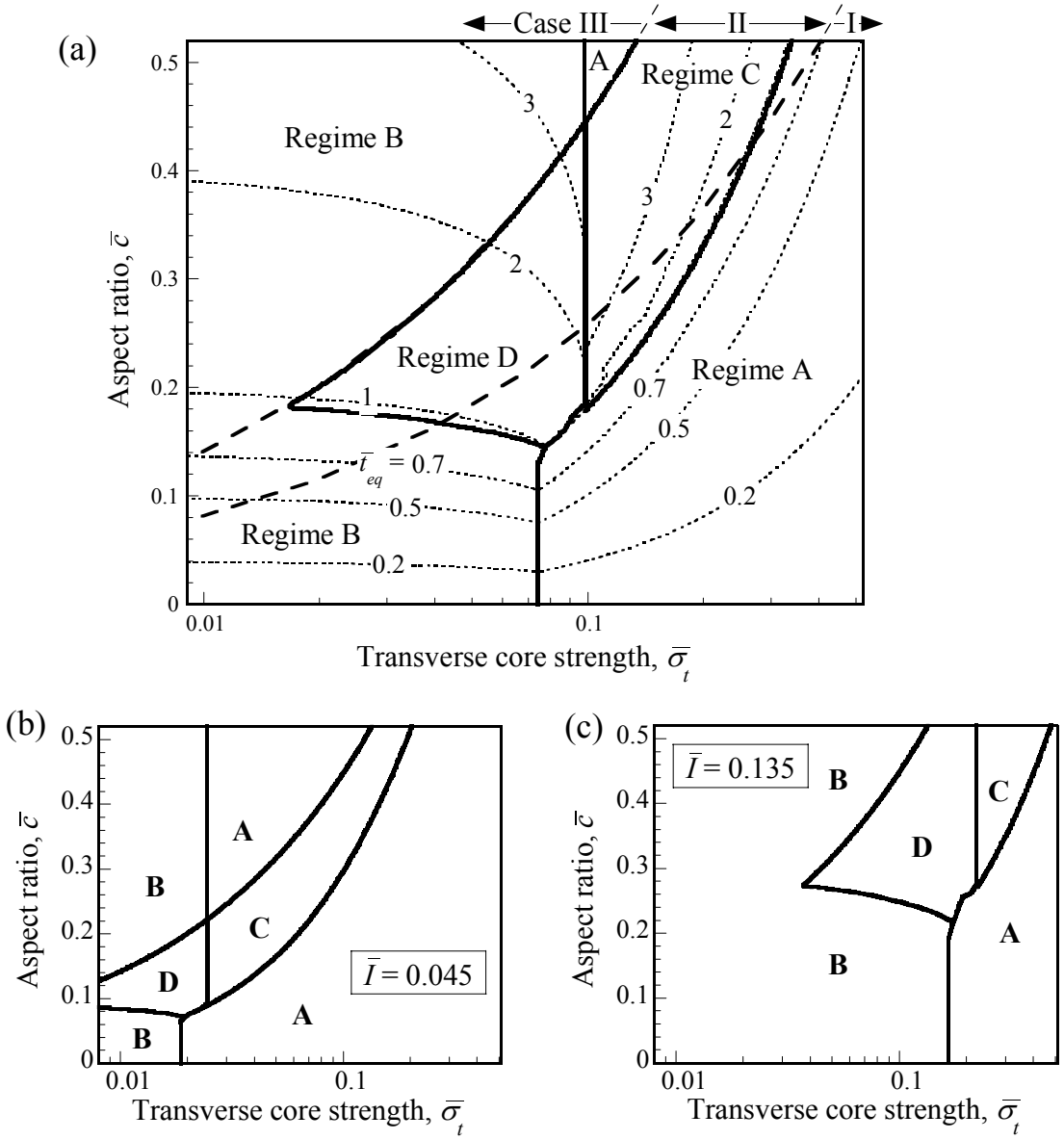

Figure 7: Maps of the regimes of behaviour of the sandwich beam with axes $\bar{c}$ and $\bar{\sigma}_t$. In these maps the beam geometrical parameters are $\bar{h} = 0.1$ and $\hat{h} = 1$ while the fixed core properties are $\bar{\rho} = 0.02$, $\varepsilon_D = 0.85$ and $\bar{\sigma}_l = 1$. (a) Map for an impulse $\bar{I} = 0.09$ with contours of $\bar{t}_{eq}$ included. The effect of the impulse $\bar{I}$ on the regime boundaries for (b) $\bar{I} = 0.045$ and (c) $\bar{I} = 0.135$.

41

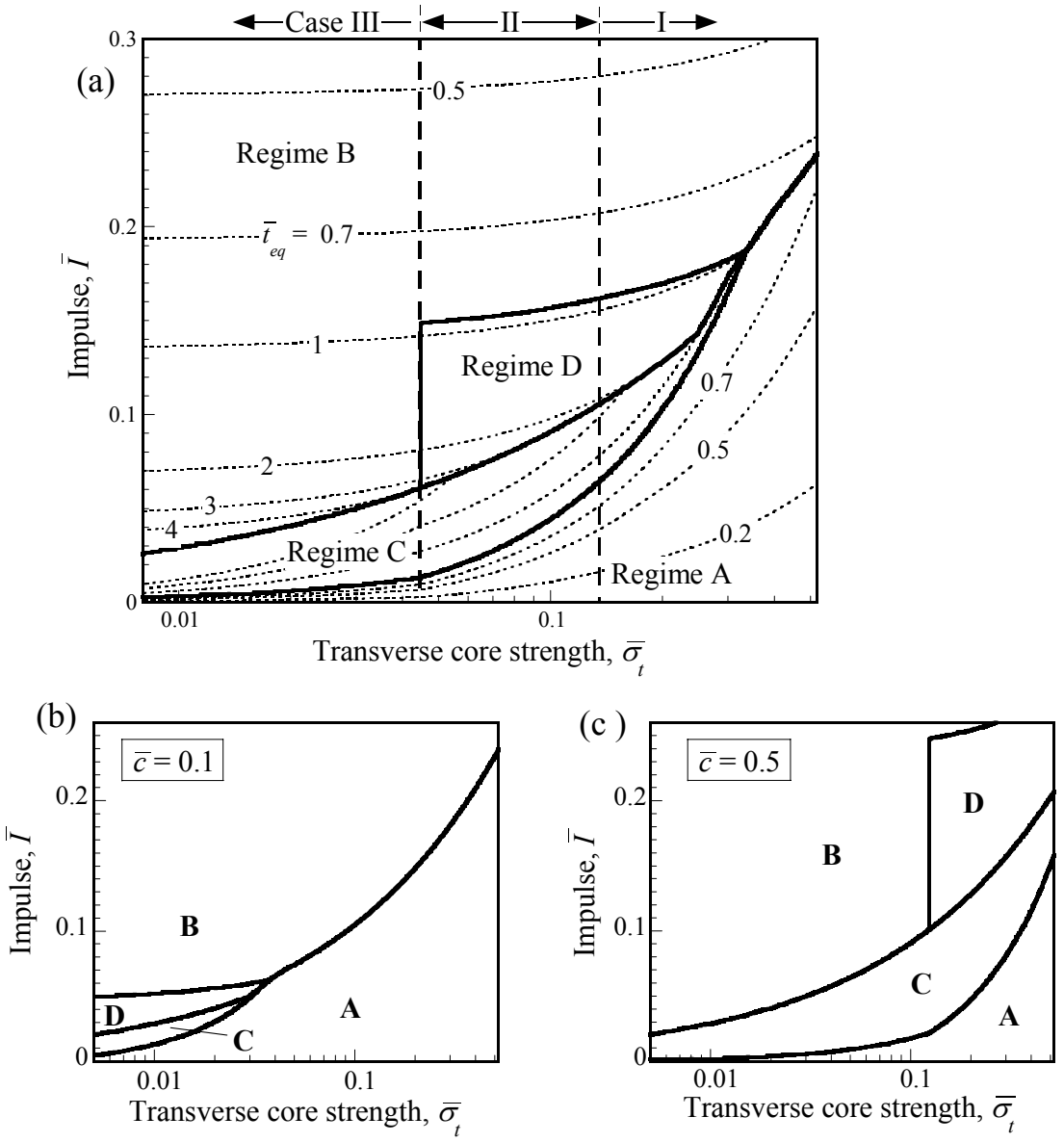

Figure 8: Maps of the regimes of behaviour of the sandwich beam with axes $\bar{I}$ and $\bar{\sigma}_t$. In these maps the beam geometrical parameters are $\bar{h} = 0.1$ and $\hat{h} = 1$ while the fixed core properties are $\bar{\rho} = 0.02$, $\varepsilon_D = 0.85$ and $\bar{\sigma}_l = 1$. (a) Map for a sandwich beam with $\bar{c} = 0.3$ including contours of $\bar{t}_{eq}$. The effect of the sandwich beam aspect ratio on the regime boundaries for (b) $\bar{c} = 0.1$ and (c) $\bar{c} = 0.5$.

42

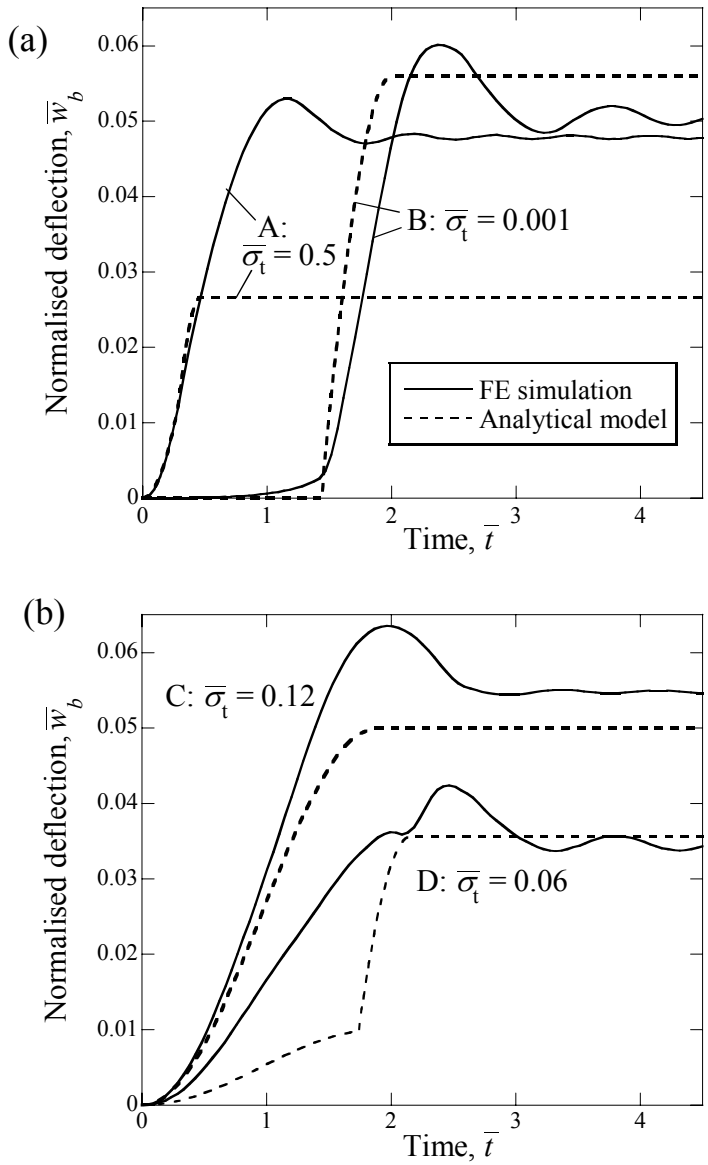

Figure 9: Analytical and FE predictions of the normalised mid-span back face deflection $\overline{w}_b$ versus time histories for sandwich beams in (a) the decoupled regimes A and B and (b) in the coupled regimes C and D. Results are shown for sandwich beams with $\overline{c} = 0.3$ subject to an impulse $\overline{I} = 0.09$ and representative values of core strength $\overline{\sigma}_t$ for each regime, as labelled. All other properties of the sandwich beam are fixed at the reference values, i.e. beam geometry $\overline{h} = 0.1$, $\hat{h} = 1$ and core properties $\overline{\rho} = 0.02$, $\varepsilon_D = 0.85$ and $\sigma_l = \tau_c = \overline{\rho}\sigma_Y$.

43

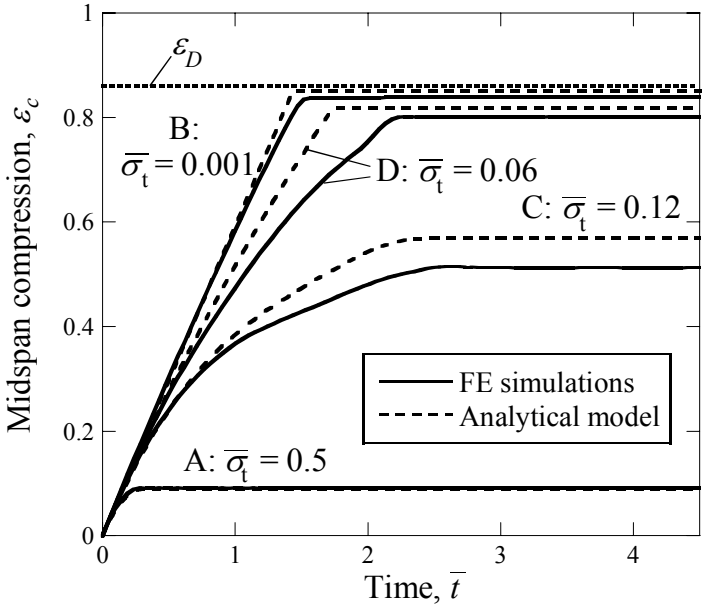

Figure 10: Analytical and FE predictions of the mid-span core compression ε_c versus time histories. Results are shown for sandwich beams with $\overline{c} = 0.3$ subject to an impulse $\overline{I} = 0.09$ and representative values of core strength $\overline{\sigma}_t$ for each regime, as labelled. All other properties of the sandwich beam are fixed at the reference values, i.e. beam geometry $\overline{h} = 0.1$, $\hat{h} = 1$ and core properties $\overline{\rho} = 0.02$, $\varepsilon_D = 0.85$ and $\sigma_l = \tau_c = \overline{\rho}\sigma_Y$.

44

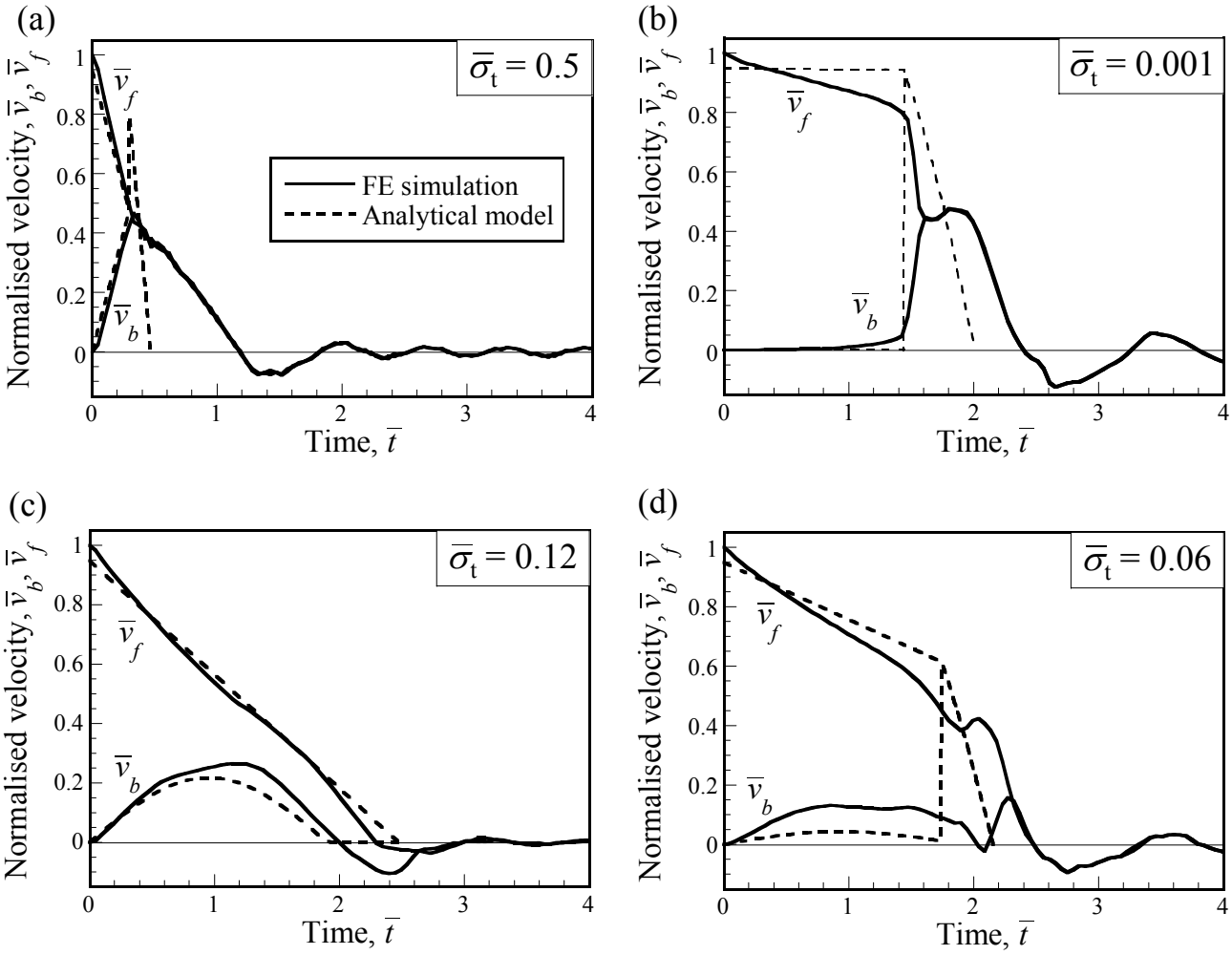

Figure 11: Analytical and FE predictions of the normalised mid-span front and back face-sheet velocity versus time histories for sandwich beams with $\bar{c} = 0.3$ subject to an impulse $\bar{I} = 0.09$. All other properties of the sandwich beam are fixed at the reference values, i.e. beam geometry $\bar{h} = 0.1$, $\hat{h} = 1$ and core properties $\bar{\rho} = 0.02$, $\varepsilon_D = 0.85$ and $\sigma_l = \tau_c = \bar{\rho}\sigma_Y$. (a) Regime A with $\bar{\sigma}_t = 0.5$, (b) regime B with $\bar{\sigma}_t = 0.001$, (c) regime C with $\bar{\sigma}_t = 0.12$ and (d) regime D with $\bar{\sigma}_t = 0.06$.

45

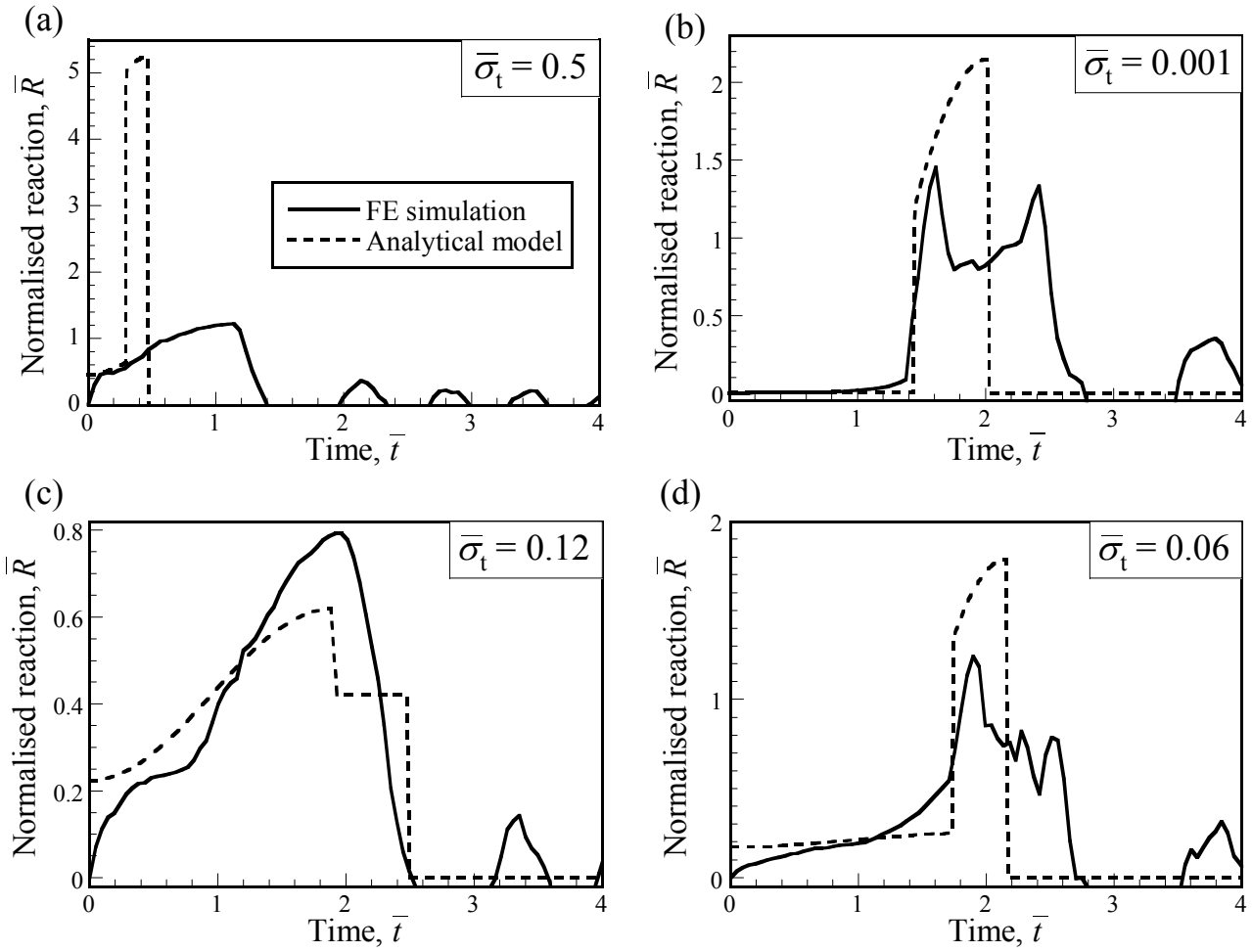

Figure 12: Analytical and FE predictions of the normalised support reaction versus time histories. for $\bar{c} = 0.3$ sandwich beams subject to an impulse $\bar{I} = 0.09$. All other properties of the sandwich beam are fixed at the reference values, i.e. beam geometry $\bar{h} = 0.1$, $\hat{h} = 1$ and core properties $\bar{\rho} = 0.02$, $\varepsilon_D = 0.85$ and $\sigma_l = \tau_c = \bar{\rho}\sigma_Y$. (a) Regime A with $\bar{\sigma}_t = 0.5$, (b) regime B with $\bar{\sigma}_t = 0.001$, (c) regime C with $\bar{\sigma}_t = 0.12$ and (d) regime D with $\bar{\sigma}_t = 0.06$.

46

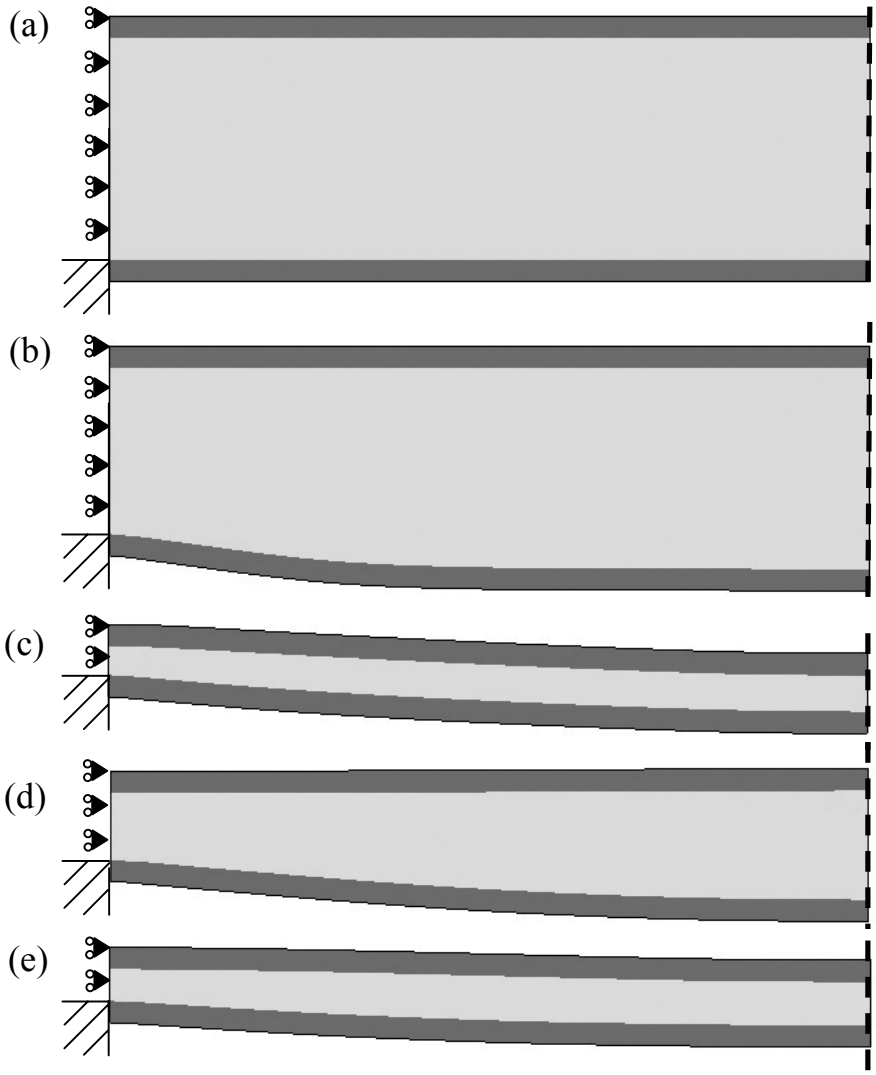

Figure 13: Finite element predictions of the (a) initial and (b-e) final deformed profiles of sandwich beams with $\bar{c} = 0.3$ subject to an impulse $\bar{I} = 0.09$. (b) Regime A with $\bar{\sigma}_t = 0.5$, (c) regime B with $\bar{\sigma}_t = 0.001$, (d) regime C with $\bar{\sigma}_t = 0.12$ and (e) regime D with $\bar{\sigma}_t = 0.06$. All other properties of the sandwich beam are fixed at the reference values, i.e. beam geometry $\bar{h} = 0.1$, $\hat{h} = 1$ and core properties $\bar{\rho} = 0.02$, $\varepsilon_D = 0.85$ and $\sigma_l = \tau_c = \bar{\rho}\sigma_Y$.

47

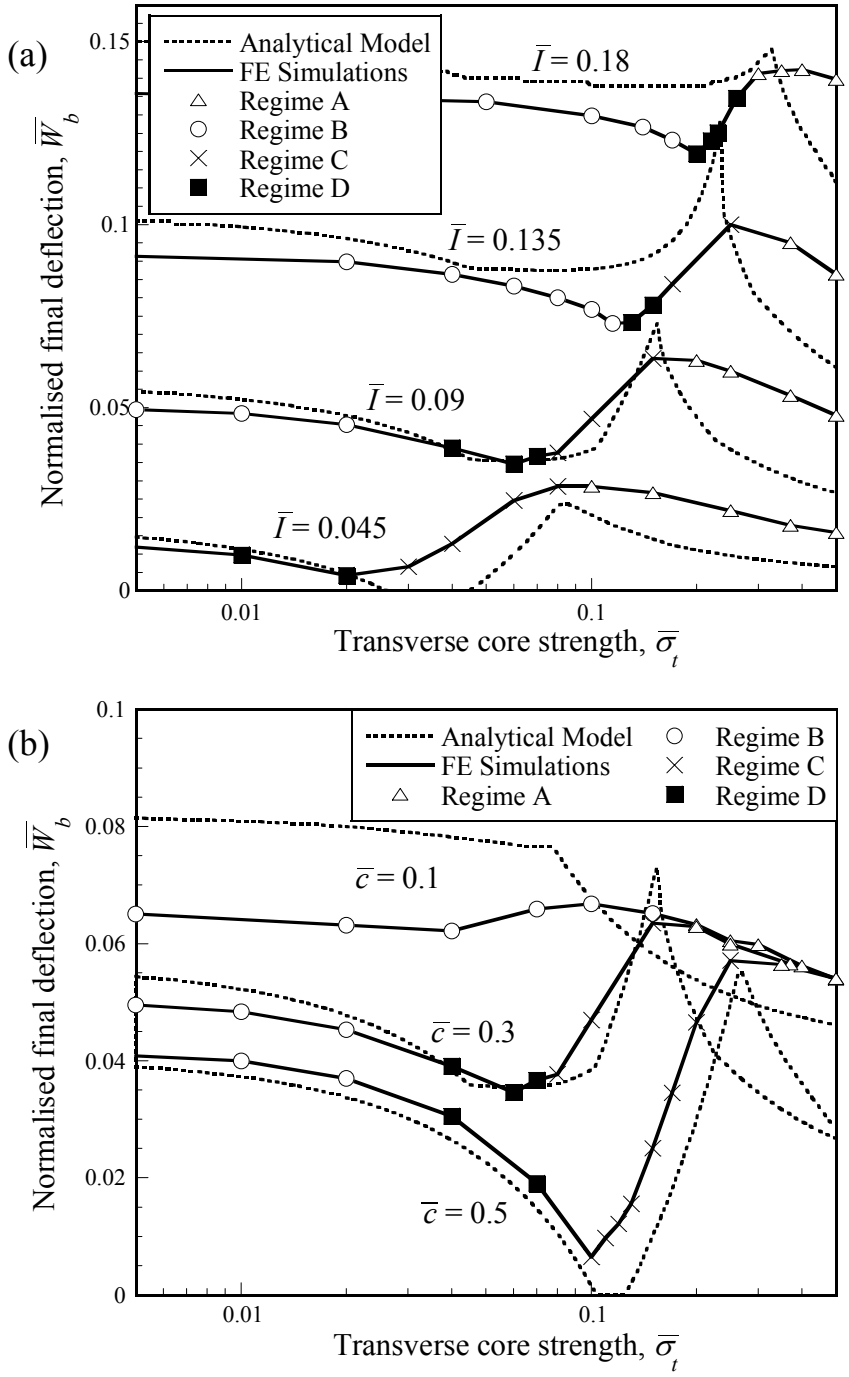

Figure 14: Comparison between analytical and FE predictions of the normalised permanent mid-span back face deflections for a range of transverse core strengths $\bar{\sigma}_t$. (a) Sandwich beams with $\bar{c} = 0.3$ for four selected values of the impulse $\bar{I}$. (b) Sandwich beams subject to an impulse $\bar{I} = 0.09$ for three selected values of $\bar{c}$. All other properties of the sandwich beam are fixed at the reference values, i.e. beam geometry $\bar{h} = 0.1$, $\hat{h} = 1$ and core properties $\bar{\rho} = 0.02$, $\varepsilon_D = 0.85$ and $\sigma_l = \tau_c = \bar{\rho}\sigma_Y$.

48

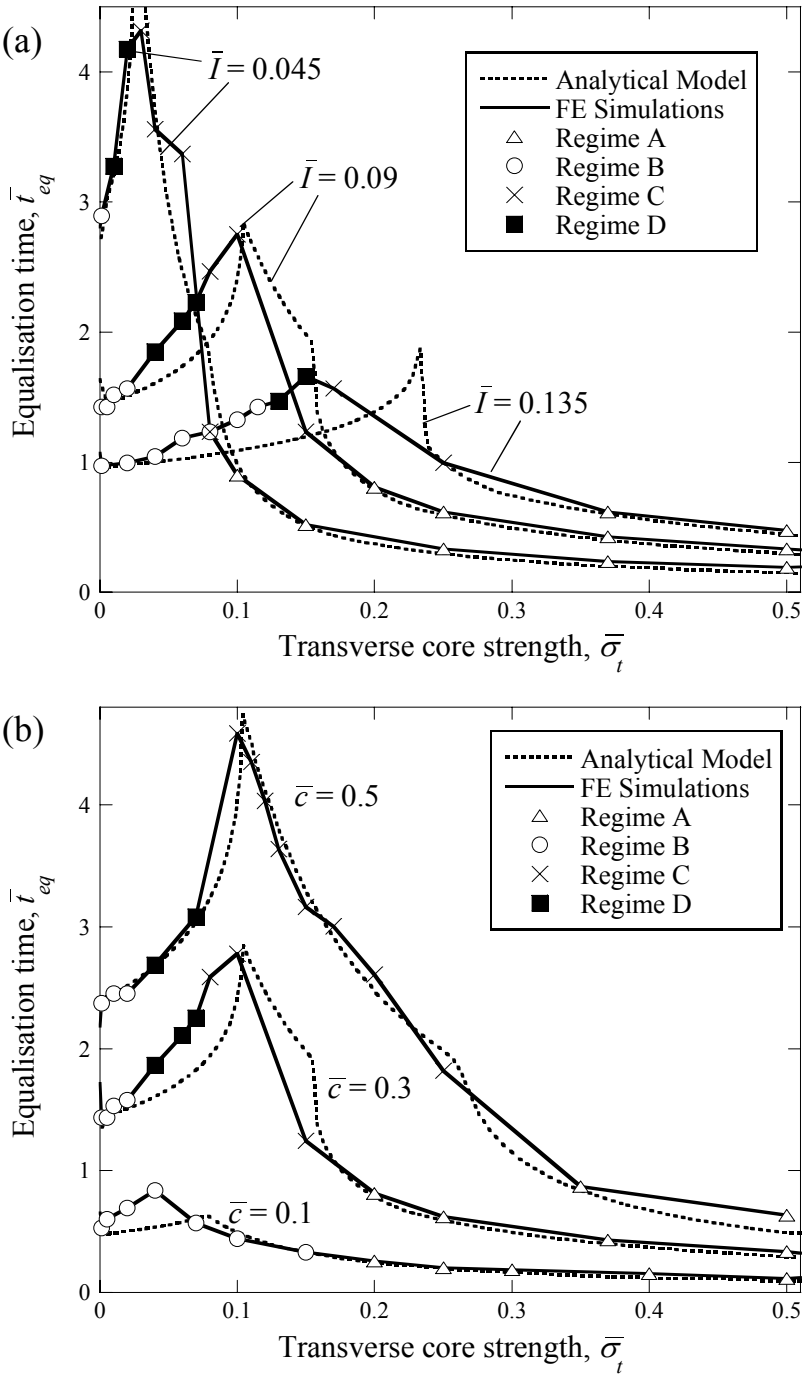

Figure 15: Comparison between analytical and FE predictions of the normalised core compression duration $\bar{t}_{eq}$ for a range of transverse core strengths $\bar{\sigma}_t$. (a) Sandwich beams with $\bar{c} = 0.3$ for three selected values of the impulse $\bar{I}$. (b) Sandwich beams subject to an impulse $\bar{I} = 0.09$ for three selected values of $\bar{c}$. All other properties of the sandwich beam are fixed at the reference values, i.e. beam geometry $\bar{h} = 0.1$, $\hat{h} = 1$ and core properties $\bar{\rho} = 0.02$, $\varepsilon_D = 0.85$ and $\sigma_l = \tau_c = \bar{\rho}\sigma_Y$.

49

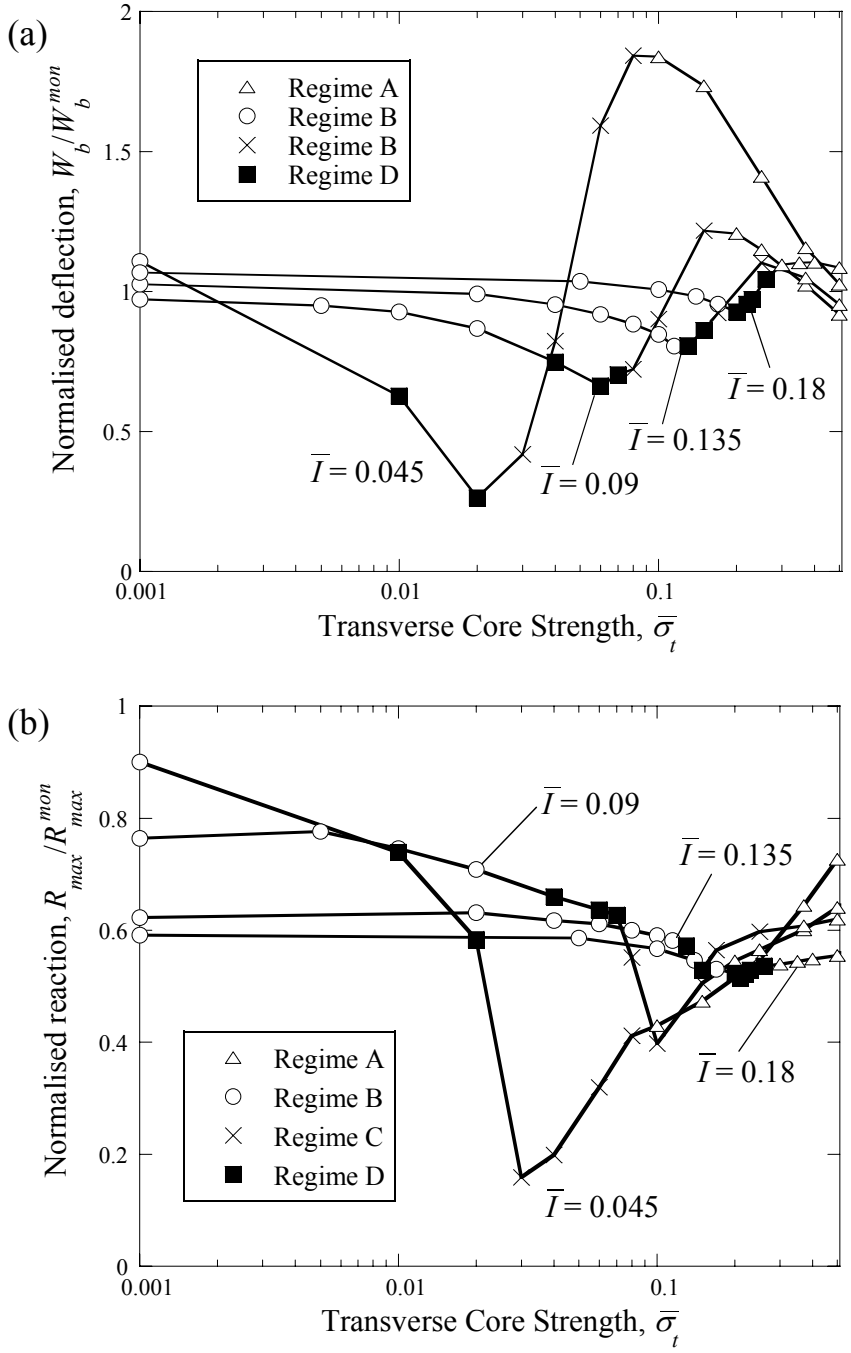

Figure 16: Finite element predictions comparing the performance of sandwich beams with $\bar{c} = 0.3$ and monolithic beams of equal mass. (a) The permanent mid-span back face deflections and (b) peak support reactions forces of sandwich beams normalised by that of monolithic beams of equal mass for four selected values of the impulse $\bar{I}$. Predictions are shown for a range of transverse core strengths $\bar{\sigma}_t$. All other properties of the sandwich beam are fixed at the reference values, i.e. beam geometry $\bar{h} = 0.1$, $\hat{h} = 1$ and core properties $\bar{\rho} = 0.02$, $\varepsilon_D = 0.85$ and $\sigma_l = \tau_c = \bar{\rho}\sigma_Y$.

50

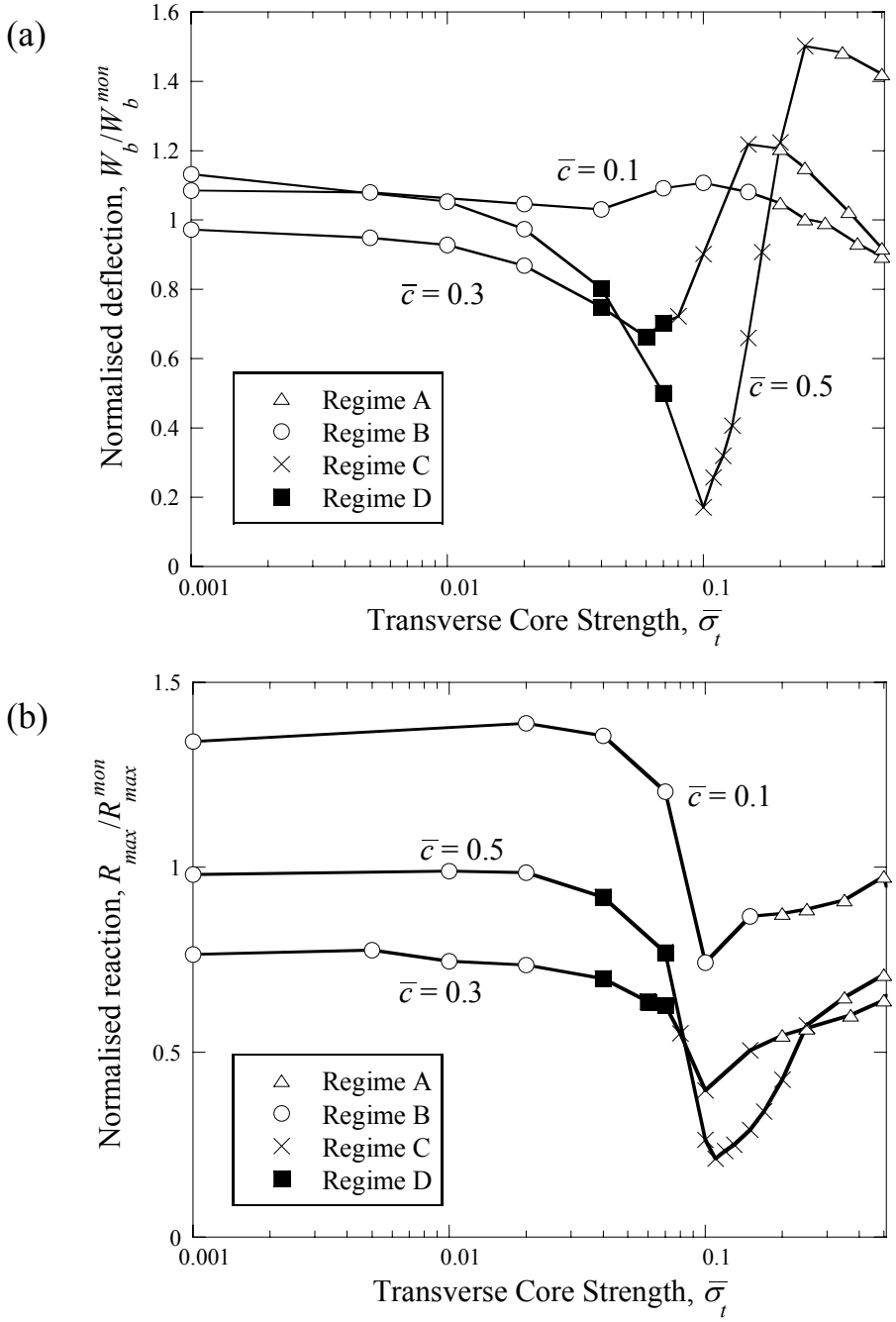

Figure 17: Finite element predictions comparing the performance of sandwich beams with monolithic beams of equal mass subject to an impulse $\bar{I} = 0.09$. (a) The peak mid-span back face deflections and (b) peak support reactions forces of sandwich beams normalised by that of monolithic beams of equal mass for three selected values of the sandwich beam slenderness ratio $\bar{c}$. Predictions are shown for a range of transverse core strengths $\bar{\sigma}_t$. All other properties of the sandwich beam are fixed at the reference values, i.e. beam geometry $\bar{h} = 0.1$, $\hat{h} = 1$ and core properties $\bar{\rho} = 0.02$, $\varepsilon_D = 0.85$ and $\sigma_l = \tau_c = \bar{\rho}\sigma_Y$.

51

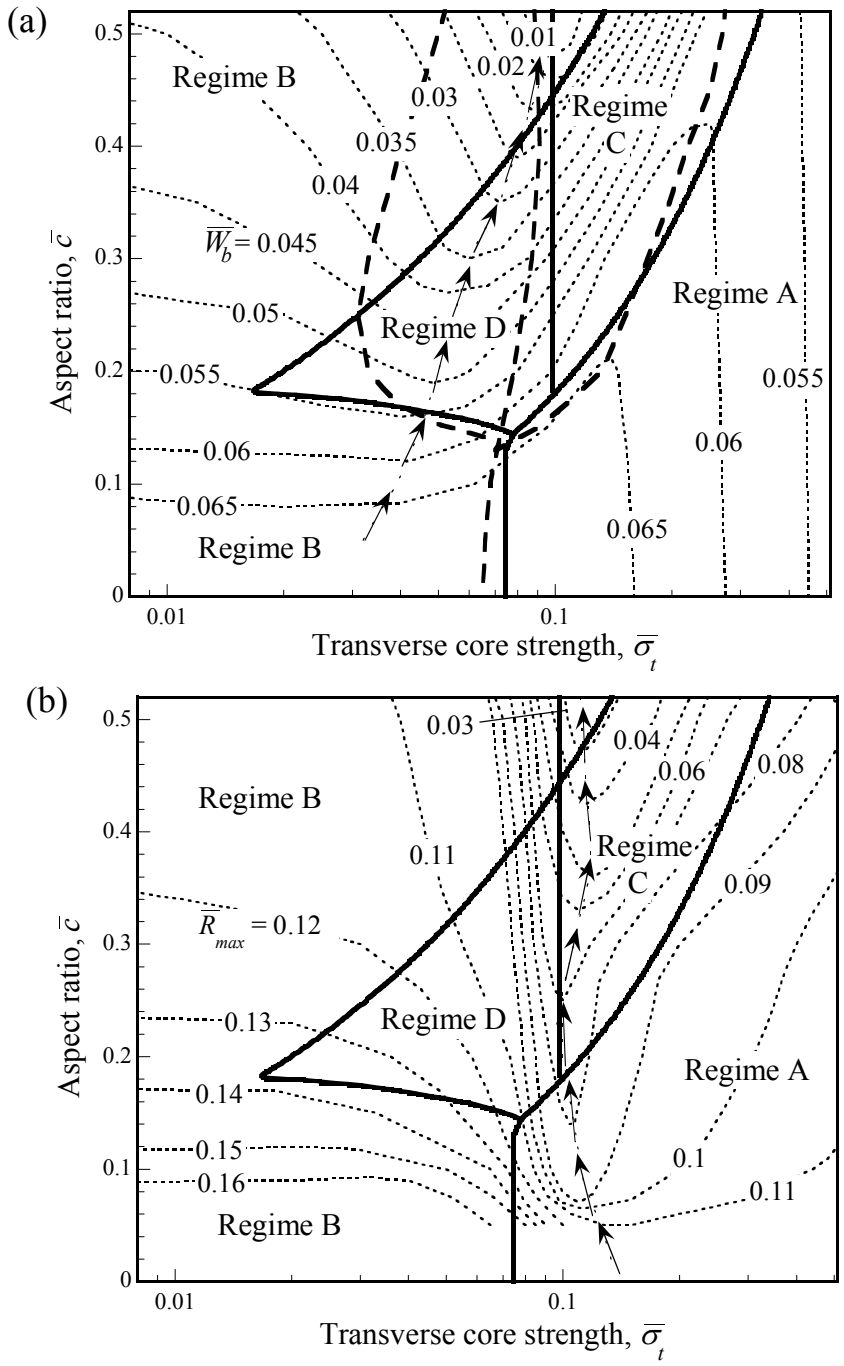

Figure 18: Design charts for sandwich beams with axes $\bar{c}$ and $\overline{\sigma}_t$ constructed for a blast impulse $\bar{I} = 0.09$. (a) FE predictions of the contours of the normalised permanent mid-span back face deflections $\overline{W}_b$. The FE (dashed lines) and analytical (thick solid lines) predictions of the regime boundaries are included. (b) FE predictions of the contours of the normalised peak support reaction force $\overline{R}_{\max}$. In these charts the fixed beam geometrical parameters are $\bar{h} = 0.1$ and $\hat{h} = 1$ while the fixed core properties are $\overline{\rho} = 0.02$, $\varepsilon_D = 0.85$ and $\sigma_l = \tau_c = \overline{\rho}\sigma_Y$. The arrows in (a) and (b) trace the path of designs that minimize $\overline{W}_b$ and $\overline{R}_{\max}$ respectively, for a given $\bar{c}$.

52

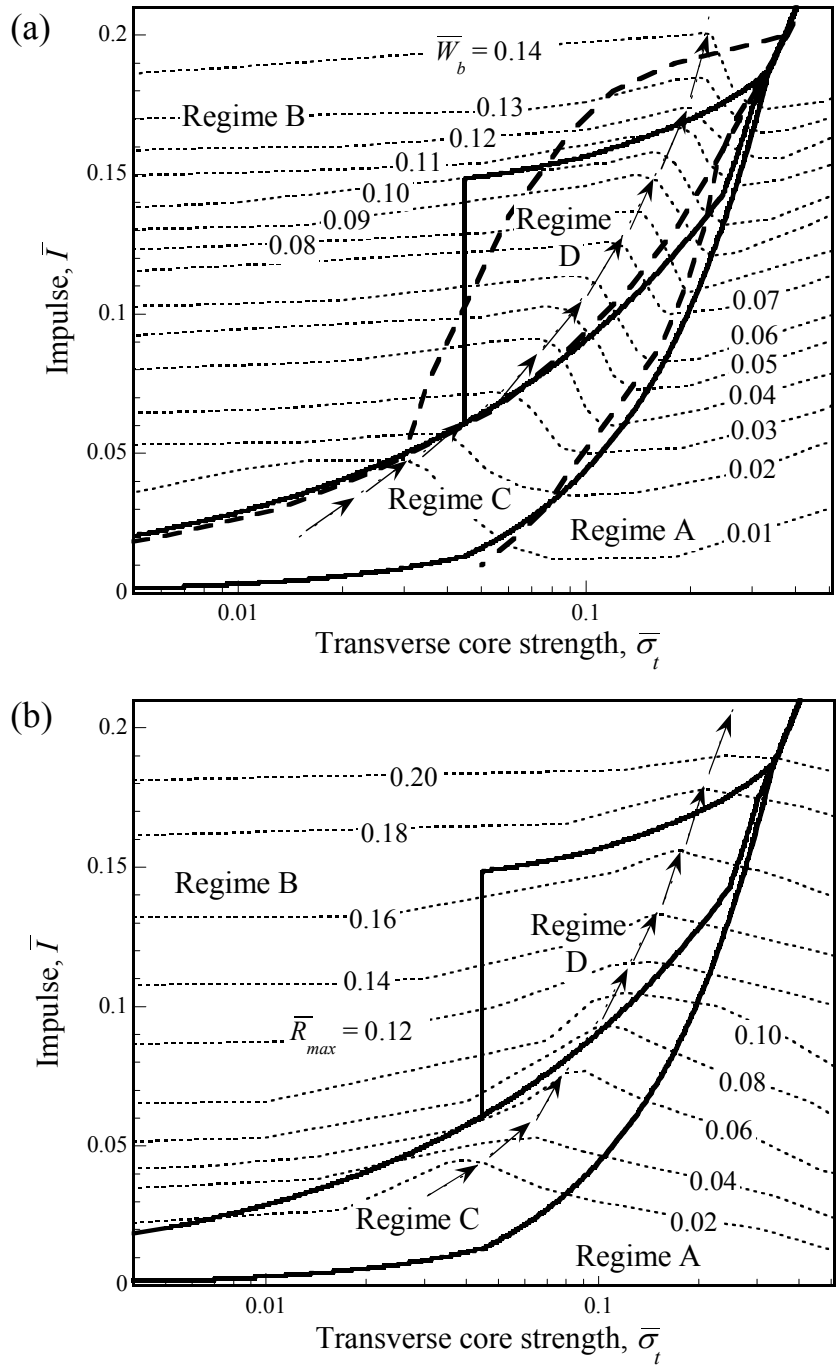

Figure 19: Design charts for $\bar{c} = 0.3$ sandwich beams with axes $\bar{I}$ and $\bar{\sigma}_t$. (a) FE predictions of the contours of the normalised permanent mid-span back face deflections $\overline{W}_b$. The FE (dashed lines) and analytical (thick solid lines) predictions of the regime boundaries are also included. (b) FE predictions of the contours of the normalised peak support reaction force $\overline{R}_{\max}$. In these charts the fixed beam geometrical parameters are $\bar{h} = 0.1$ and $\hat{h} = 1$ while the fixed core properties are $\bar{\rho} = 0.02$, $\varepsilon_D = 0.85$ and $\sigma_l = \tau_c = \bar{\rho}\sigma_Y$. The arrows in (a) and (b) trace the path of designs that minimize $\overline{W}_b$ and $\overline{R}_{\max}$ respectively, for a given $\bar{I}$.

53